Development of an RVE and its stiffness predictions based on mathematical homogenization theory for short fibre composites

K.P. Babu, P.M. Mohite*, C.S. Upadhyay

Department of Aerospace Engineering, Indian Institute of Technology Kanpur, UP 208016, India

A B S T R A C T

In this study an attempt is made to generate the microstructure of short fibre composites through representative volume element (RVE) approach and then analyzed using mathematical theory of homogenization with periodic boundary conditions to estimate the homogenized or effective material properties. An algorithm, based on random sequential adsorption technique (RSA), has been developed to generate the RVE for such materials. The goal of the present study is to demonstrate the methodology to generate RVEs which are effective in predicting the stiffness of the short fibre composites with repetitiveness. For this purpose, RVEs for four different scenarios of fibre orientations have been developed using this technique. These four different scenarios are: Fibres are aligned in a direction; fibres are oriented randomly in one plane; fibres are randomly oriented in one plane and partially random oriented in other plane and finally, fibres are completely random oriented. For each case three to four different fibre volume fractions are studied with five different RVEs for each volume fraction. These four cases presented different material behaviour at macroscale due to random location and orientation of fibres. The effective properties obtained from numerical technique are compared with popular non RVE methods like Halpin–Tsai and Mori–Tanaka methods for the case where fibres are aligned in a direction and were found to be in good agreement. The variation in the predicted properties for a given volume fraction of any of the four cases studied is less than 1%, which indicates the efficacy of the algorithm developed for RVE generations in repetitiveness of predicted effective properties. The four cases studied showed gradual change in macroscopic behaviour from transversely isotropic, with respect to a plane, to a nearly isotropic nature.

© 2017 Elsevier Ltd. All rights reserved.

1. Introduction

Materials selection and their properties plays a primary role in engineering design. The performance of the structure or component relies mainly on the material properties. Fibre reinforced composites (FRC) made with polymer matrix materials are popular materials due to their high specific stiffness, strength, toughness and fatigue behaviour. Fibre reinforced composites, with long fibres, processed by cost effective manufacturing techniques are efficient to carry primary loads, but there are many applications for which the requirements are less demanding and the expensive manufacturing techniques cannot handle long fibres due to complexity of shape. Therefore, in such situations short fibre reinforced composites (SFRC) are widely used (Harris, 1999). SFRC products are commonly manufactured by conventional manufacturing techniques like injection moulding, compression moulding and extrusion processes, etc. However, injection moulding process

is a popular method used in industries for manufacturing polymeric composites of complex shapes without compromising the performance of components at a reasonable cost. During the manufacturing process, molten polymer along with short fibres is injected into the mould followed by curing process and the final part is extracted from the mould (Vincent et al., 2005; Park and Park, 2011). SFRCs obtained from injection mould technique are widely used in auto-mobile and civil engineering applications because of their less weight and increased production rates. Recent applications of SFRCs in aerospace domains include replacement of metallic structures to carry enough loads due to secondary loading members (Rezaei et al., 2009). To expand their applications in various sectors, prediction of material behaviour is essential. Short fibre composites are being extensively used in automotive structural applications due to their low costs and mass production capabilities. However, to extend its application in aerospace domain, the material behaviour needs to be analyzed carefully.

The material properties of short fibre reinforced composites depend upon many criteria apart from their individual constituent properties. The factors such as volume fraction, fibre orientation,

* Corresponding author.
  E-mail address: mohite@iitk.ac.in (P.M. Mohite).

fibre location, fibre aspect ratio, cross sectional geometry of fibre and size of RVE decide the properties of resulting material. These criteria have to be considered while predicting the properties of short fibre composites. This leads to a challenging task. The different methods used to predict the properties of SFRCs are analytical or non RVE methods, micromechanics based finite element method using homogenization techniques and Fast Fourier Transform technique.

To investigate the material behaviour of SFRCs, different analytical methods are available in literature. The most popular methods are (Mori and Tanaka, 1973) and (Halpin, 1969; Halpin and Kardos, 1976) techniques. Mori and Tanaka (1973) technique is based on Eshelby's (1957) inclusion in isotropic medium to estimate the average internal stress in a matrix containing inclusion with eigenstrain. Mori–Tanaka method does not derive the explicit relations for the effective stiffness tensor of composite. Later, Benveniste (1987) reconsidered and proposed a closed form expression to compute the effective moduli based on the assumption that the average strain in inclusion is related to average strain in matrix material by a fourth order tensor. This fourth order tensor relates uniform strain in the inclusion embedded in matrix material, subjected to uniform strain at infinity. Chow (1978); Tucker and Liang (1999) proposed an expression for strain concentration tensor based on dilute Eshelby's model and average strain in matrix, to predict the stiffness tensor of short fibre composites.

Among numerical approaches, Ionita and Weitsman (2006) developed a material model for SFRCs which simulates the random geometry of material based on laminated random strand technique to predict the material properties. This method is based on classical laminate theory where the fibres are randomly oriented in in-plane and does not account for out of plane orientation of fibres. Nazarenko et al. (2016) developed a mathematical model based on energy-equivalent homogeneity combined with the method of conditional moments to analyse short fibre composites. The parallel and random distribution of fibres was considered and the interphase was described by Murdoch material surface model. The properties of the energy-equivalent fibre are determined on the basis of Hill's energy equivalence principle assuming its cylindrical shape.

Approaches using finite element method, as a numerical tool, to compute the material behaviour of SFRCs are very popular. Kari et al. (2007) developed the RVE models based on the numerical technique to estimate the material behaviour of random short fibre composites. They studied the influence of size effect on RVE considering both the constituents as isotropic in nature. Velmurugan et al. (2014) estimated the effect of material behaviour influenced by unidirectionally aligned curved short fibre composites for glass/epoxy composites and aluminum/boron composites. In their study, curved fibres of sinusoidal shape were considered and characterized by amplitude, wavelength and diameter of fibre. Jain et al. (2013) developed the microstructure model known as volume element using random sequential algorithm (RSA) (2007) to predict the stresses in individual inclusion and matrix material. The fibres were modeled as sphero-cylinders and ellipsoids of various aspect ratios. Further, fibres were allowed to be unidirectionally aligned and also randomly oriented in in-plane. Fully random orientation of fibres was not considered in their study. Fu and Lauke (1996) developed an analytical method considering the effects of fibre length and fibre orientation distributions for predicting the tensile strength of short fibre reinforced polymers. The strength of these polymers is derived as a function of fibre length and fibre orientation distribution taking into account the dependences of the ultimate fibre strength and the critical fibre length on the inclination angle and the effect of inclination angle on the bridging stress of oblique fibres.

Ghossein and Lévesque (2012) developed a numerical tool to predict the effective properties of composites by generating RVE with randomly distributed spherical particles as reinforcement using an algorithm based on molecular dynamics. Duschlbauer et al. (2006) developed an RVE by using Monte Carlo algorithm to estimate the thermoelastic and thermophysical behaviour of metal matrix composites. In their study, the fibres were oriented randomly in in-plane direction. Eckschlager et al. (2002) also implemented the unit cell approach for metal matrix composite to study the elastic behaviour of random oriented discontinuous fibre reinforcements. Spherical and cylindrical fibre reinforcements were generated using RSA algorithm for 15% volume fraction. A finite element implementation of these models was done using ABAQUS. Doghri and Tinel (2005) proposed an RVE development using orientation distribution function and averaging is pronounced in two steps. Firstly, homogenization of each pseudo grain is obtained. Secondly, homogenization of all pseudo grains is done to estimate the macro response of RVE. Numerical simulations were performed on elasto-plasto matrix components known as silicon fibre reinforced aluminum alloy. Pan et al. (2008a) developed a numerical technique to generate the microgeometry using RSA technique to estimate the effective properties of short fibre reinforced composites. Glass fibres were modeled with an elliptical cross sectional shape and large volume fraction is obtained by allowing the fibres to bend sharply over the other fibres at the crossing region, which leads to a high stress concentration in the kink region of fibres. They also addressed the fibre interaction effect on local stress field by varying the distance between two fibres. Advani and Tucker (1987) applied the use of even order orientation tensors to study the effect of orientation on unidirectional aligned composites. Ogierman and Kokot (2016) studied the fibre orientation and its influence on material properties and dynamic response of the structure based on the coupling of injection moulding technique to distribute the short fibres, microscale modeling to represent an RVE and finite element based homogenization technique to estimate the material properties. Orientation averaging approach proposed by Advani and Tucker (1987) is considered to couple the fibre orientation data obtained from injection moulding technique and to estimate the effective properties. Berger et al. (2007) evaluated the effective properties of randomly distributed cylindrical fibre composites. They used numerical homogenization tool for this purpose. Their focus was to study the influence of change in volume fraction and length/diameter aspect ratio of fibres. In their study they considered arbitrarily oriented and parallel oriented fibre arrangements.

Most of the works based on some homogenization technique depend on the size of an RVE. In the present study, a micromechanics model based on mathematical theory of homogenisation is implemented to determine the effective properties. This approach is independent of the size of RVE. RVE development plays a key role in finite element procedure to determine the effective properties of the material.

The behaviour of a composite material can be predicted by studying the effect of its individual constituents at microscale. The arrangement of fibres in matrix plays a vital role in the development of a model for this study. The assumptions made for a typical micromechanics analysis can be seen in the work of Hori and Nemat-Nasser (1999). A square packed fibre and matrix arrangement is popularly used model to represent the microscale model of continuous fibre composites as shown in Fig. 1(a) (shown as an example). Due to symmetry and periodic arrangement of fibres, a single rectangular array can be used to analyse the material at microscale which is known as representative volume element (RVE). Similarly, a random packing and periodic arrangement of fibre and matrix at microscale indicates a RVE for short fibre composites. A sample RVE (in 2D) for short fibre composite is shown in Fig. 1(b).
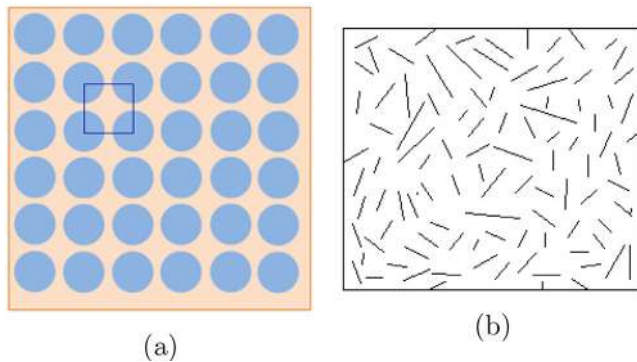
Fig. 1. Representative volume elements for continuous and short fibre composites. (a) RVE for continuous fibre composite, (b) RVE for short fibre composite.

The characterization of a composite material structure is studied using RVE at the microlevel, which decouples the composite analysis into macro and micro level analyses. Microstructural details are considered in local level analysis to determine the effective properties and to calculate the relationship between effective or average RVE strain and the local strain within the RVE. In global level analysis, the actual composite structure is replaced by an equivalent homogenized material having the calculated effective properties to determine the average stress and strain within equivalent homogenized structure (Hollister and Kikuchi, 1992). Sukiman et al. (2017) studied a microstructure of randomly distributed short fibre composites using computational homogenization to evaluate effective thermal and mechanical properties. The focus of the work was to study the effect of area fraction on the size of the deterministic representative volume element (DRVE). This study was based on two dimensional RVE.

Determination of RVE size is an important aspect for RVE based methods. In general, the RVE must be chosen such that the requirements of statistical homogeneity must be satisfied by the RVE so as to provide a meaningful statistical representation of typical material properties. Iorga et al. (2008) proposed a method based on laminated random strand method for RVE size. This method is well suited for the composites with randomly oriented in-plane fibres. Pelissou et al. (2009) proposed a statistical strategy for RVE size determination for a metal matrix composite with randomly distributed aligned brittle inclusions. The work carried out by Gitman et al. (2007) can be seen, as an example, for more details on existence and size determination of RVE. One can also see the study of Kanit et al. (2006) for the estimation of RVE size.

The main objective of this article is to automatically develop an RVE of short fibre composites and estimate its effective properties through micromechanical models. Here, random sequential adsorption technique proposed by Pan et al. (2008b) is implemented in a numerical method to generate the RVE for chopped fibre composites. The mathematical theory of homogenization (Hollister and Kikuchi, 1992) is used to predict the effective properties of RVEs developed. Furthermore, the homogenization method is implemented in a finite element code with periodic boundary conditions. This is implemented through the periodic nature of RVEs generated. Thus, the overall goal is to develop an approach to generate the microstructure of short fibre composite and predict its effective macroscopic behaviour. Further, the approach should be efficient in predicting the properties repetitively for a given scenario. The detailed procedure implemented to make the RVEs periodic in nature is also presented. In the present study, different scenarios of RVEs have been generated to study the effect of fibre orientations on the effective properties. Here, the following four types of RVEs are generated and studied for the effective behaviour.

Case 1: Fibres are aligned in a direction.
Case 2: Fibres are randomly oriented in one plane.
Case 3: Fibres are randomly oriented in one plane and a small deviation is allowed in one of the remaining plane.
Case 4: Fibres are completely randomly oriented in all planes.

Furthermore, the effect of fibre volume fraction on the effective properties of the RVEs of all four cases is also studied. For each of the case, three fibre volume fractions are studied and for each volume fraction five RVEs are generated and analyzed for effective properties.

The novelty of the current study is to give a simple methodology, using RSA technique to generate the RVE with periodicity of the material for short fibre composites. Here, the emphasis is given on the generation of 3D RVEs rather than 2D RVEs for better interaction effect of surrounding fibres. A detailed methodology to ensure the material periodicity across all boundaries of the cuboid RVE has been presented. Further, a suitable homogenization procedure is used such that for a given type of fibre distribution the effective properties from different RVEs are predicted consistently. This has been demonstrated through numerous simulations over different RVEs as mentioned above.

In the following section, the methodology adopted for the generation of RVEs is presented in detail. Thereafter, the efficacy of the generated RVEs presenting different types of composites is demonstrated through their effective properties. The effective properties of these RVEs are predicted by mathematical theory of homogenization (Hollister and Kikuchi, 1992). The theory is implemented through a finite element code. The finite element formulation of the theory is also presented briefly. Finally, the effective properties of the resulting composites are analyzed and presented.

Remark 1. The development of an approach for RVE generation for short fibre composite and its effective behaviour prediction can easily be applied to multi-scale CNT (Carbon Nano-Tube) composites analysis. The effective Carbon nano-fibre can be obtained either from molecular dynamics or from micro-mechanics technique like Concentric Cylinder Assemblage (CCA) model of Hashin and Rosen (1964). The details of this work can be seen in Seidel and Lagoudas (2006). Here, the effective CNT fibres can be used as short fibre in the RVE. The present work is a link aimed for such a multi-scale analysis.

2. Generation of RVE

In determining the effective properties of composite materials using finite element technique, the generation of RVE plays a vital role. In the present study the size of the cuboid shape RVE is chosen following the work of Iorga et al. (2008). The size of the RVE is based on laminated random strand method. It takes into account the length and diameter (aspect ratio) of fibres. Further, the thickness dimension of the RVE is chosen based on pseudo-layers of the stands. More details can be seen in Iorga et al. (2008) and references therein. One can see the work of Gitman et al. (2007) for the various definitions of an RVE used in literature as well its size determination.

In this section, steps involved in the generation of an RVE with geometric periodicity is explained in the following.

2.1. Random sequential adsorption technique

Random sequential adsorption technique is widely employed to generate the representative volume element to study the elastic properties of random chopped fibre composites. In the following, we briefly explain the working of this technique.
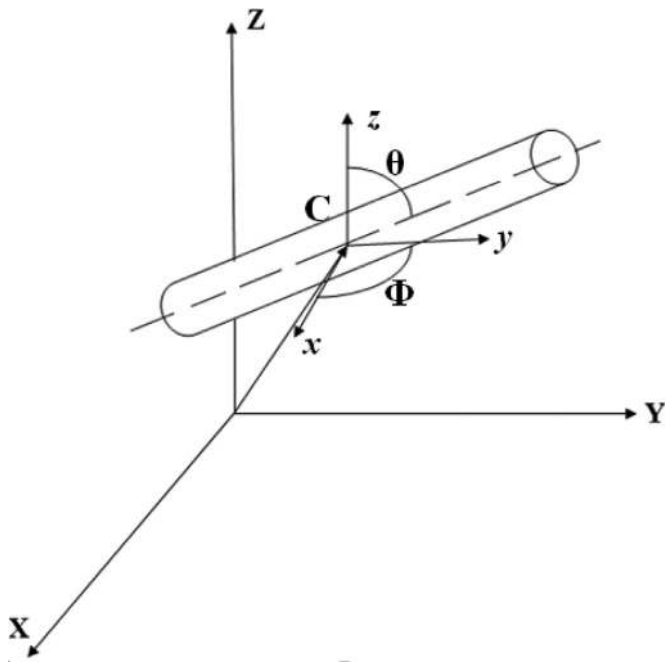
Fig. 2. Fibre model in a 3D space (Iorga et al., 2008).

In a 3D space, chopped fibre is modeled as a straight cylinder with its center point C, radius r, length l, in-plane orientation angle Φ and out-of-plane orientation angle θ, as shown in Fig. 2.

The random sequential adsorption algorithm for RVE generation deposits fibres sequentially into the cube by randomly generating their center points C and two Euler angles. Here, the location and orientations are generated according to uniform probability distribution function. Practically, two fibres are not allowed to intersect each other. Further, the penetration of a new fibre with previously accepted fibre is also not allowed in RSA algorithm. The periodicity of fibre is maintained in RSA algorithm to ensure material continuity across the boundaries when multiple RVEs are arranged for the generation of macrostructure, since RVE is locally periodic. A certain minimum distance is maintained between two random fibres to avoid the generation of excessively steep stress gradients and meshing difficulties. The minimum distance in this algorithm is being set as 0.001 times the side length of RVE. The volume fraction is updated each time when a newly generated random fibre is placed inside the cube satisfying the above criteria.

2.2. Geometric periodicity

To study the behaviour of composite materials comprising of fibre and matrix, microstructural model had been generated. Microstructural model, here known as representative volume element, is a statistical representation of real structure with heterogeneous nature. One of the major assumption of RVE generation is that the model is geometrically periodic in nature. The key idea of this section is to detail the implementation of geometric periodicity in the development of RVE.

The geometric periodicity can be seen as material periodicity, that is, the material should not experience the wall effect. In other words, it means that the reinforcement should penetrate through the walls or boundaries of an RVE (see Gitman et al., 2007). In order to have the continuity of the material the reinforcements penetrating the boundaries are allowed to reappear through opposite sides. Thus, an RVE represents any part of the material and can be considered as the part of a larger sample. On similar lines, to ensure the geometric or material periodicity for a 3D (cuboid)

RVE, geometric periodicity has to be maintained all along the faces, edges and corners of RVE considered. Therefore, by replicating an RVE in three perpendicular directions one should be able to form the actual structure.

In the following sections, the implementation of periodicity across faces, edges and corners is explained in detail. A model cubic cell and its nomenclature used in the generation of geometric periodicity in an RVE is presented in Fig. 3. This nomenclature can be used for more than one cell with respect to the cell number.

2.2.1. Periodicity across faces

In this case periodicity across faces is implemented to maintain the continuity of fibres across the faces of an RVE when a fibre crosses a face. The following procedure is incorporated to build the periodicity of an RVE across face.

The fibres that are crossing the face of a parent cell is shared by a single adjacent virtual cell as shown in Fig. 4(a). The parent cell is numbered as cell 1 and virtual cell is numbered as cell 2. A part of fibre shared by cell 1 is named as region 1 and denoted as $R1$. The remaining part of fibre shared by cell 2 is named as region 2, which is denoted as $R2$. In this case, fibre crossing the face 2 of cell 1 enters the face 4 of cell 2 as shown in Fig. 4(a). The fibre is trimmed by the face across which it crosses and separated along with their respective cells as shown in Fig. 4(b). The region 1 of fibre along with cell 1 separately and region 2 of fibre along with cell 2 separately cannot be considered as an RVE, because the continuity of the fibre is not maintained across the faces of individual cells. To ensure the continuity of fibre across faces, $R2$ of cell 2 is copied to occupy the same position in cell 1 as shown in Fig. 4(c). The same can be obtained by copying $R1$ of cell 1 to occupy same position in cell 2. Now, the cell in Fig. 4(c) can be stated as an RVE. It should be noted that the common intersection between cylindrical fibre and faces of an RVE need not be circular in shape, due to orientation of fibre.

2.2.2. Periodicity across edges

This case deals with the implementation of periodicity when fibres cross the boundary of RVE through the edges. Here, a fibre is considered to pass across the edge FH in cell 1, as shown in Fig. 5(a).

A fibre crossing the edge of a parent cell is shared by three virtual adjacent cells as shown in Fig. 5(a). This part of the fibre, along with the parent cell, is not periodic in nature. The following steps are adopted to make the parent cell to be periodic.

Both parent and virtual cells along with fibre are trimmed with X and Y planes and separated as shown in Fig. 5(b). The fibre is trimmed into four different regions and named along with their respective cells as $R1$ through $R4$. Each region of fibre along with its shared cell does not make the respective cell geometrically periodic along the edges. To make periodic arrangement, part of fibres from cell 2, cell 3 and cell 4 are copied and made to occupy the same position and orientation in cell 1 as they occupied in their respective cells as shown in Fig. 5(c). The cubic cell in Fig. 5(c) can now be called as an RVE. The same RVE can be generated from any of the adjacent cell by making the regions of fibre in the remaining cell to occupy the same position in this cell.

2.2.3. Periodicity across corners

When fibres are sequentially arranged in a cube, there is a possibility that a fibre may cross the boundary of the cube through its corner. A fibre crossing the boundary of the parent cell through its corner is shared by seven adjacent virtual cells as shown in Fig. 6(a). Each cell holds a small region of fibre. The parent cell is numbered as cell 1 and the remaining cells are virtual cells and their numbering is shown in Fig. 6(a). The fibre crossing the corner of cell 1 is trimmed by X, Y and Z planes and then separated in the

Model Cell Nomenclature

ABDC - Face 1	AB - Edge 1	HG - Edge 7
BFHD - Face 2	BD - Edge 2	GE - Edge 8
FEGH - Face 3	DC - Edge 3	BF - Edge 9
EACG - Face 4	CA - Edge 4	DH - Edge 10
AEFB - Face 5	EF - Edge 5	AE - Edge 11
CGHD - Face 6	FH - Edge 6	CG - Edge 12

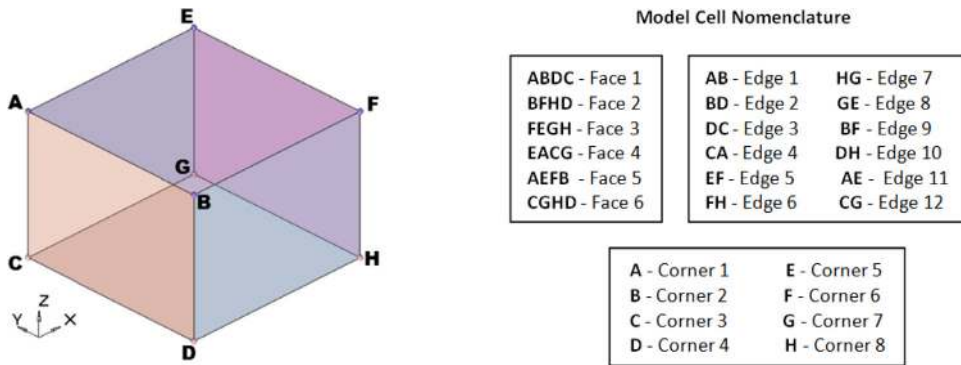| A - Corner 1 | E - Corner 5 |
B - Corner 2	F - Corner 6
C - Corner 3	G - Corner 7
D - Corner 4	H - Corner 8

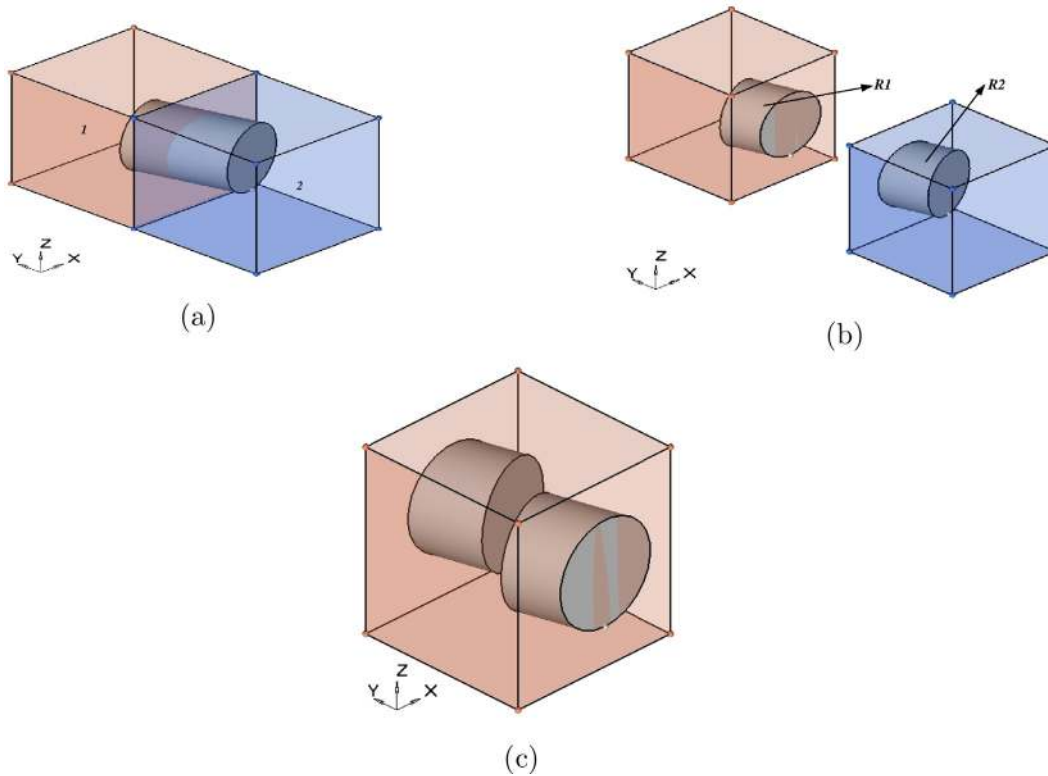**Fig. 3.** A model cell and its nomenclature in an RVE.

Fig. 4. Periodicity in an RVE with fibres across faces. (a) Fibre across a face of a unit cell, (b) trimmed fibre across a face, (c) RVE made with periodicity across faces.

respective cells as shown in Fig. 6(b). *R*1 along with cell 1 alone does not represent an RVE. To ensure it as an RVE, geometric periodicity needs to be maintained. Hence, region of fibres from seven adjacent virtual cells are copied and made to occupy the same position in the parent cell as it occupied in their respective virtual cells as shown in Fig. 6(c). Now the cell in Fig. 6(c) can be termed as an RVE with periodic arrangement across the corners. With the similar procedure, any of the virtual adjacent cell can be made an RVE with periodicity across the corners.

Remark 2. In an actual RVE, the periodicity will include the periodicity across all faces, edges and corners.

2.3. Mathematical formulation for line intersection

In the generation of RVE, the fibres are added sequentially until the required volume fraction is attained. In addition, the new fibre added should not intersect with the previously added fibres. Thus, an algorithm to check for the intersection of fibres is required. An algorithm has been developed using Sunday's technique

(Schneider and Eberly, 2002) to check the intersection of two fibres using calculus. The fibres considered are straight and cylindrical in shape. So, to check for intersection it is easy to check the distance between two axes of cylinders rather than comparing the distance between two surfaces of the cylinders.

Consider two lines L_1 and L_2 given as, respectively

$$\vec{P}(s) = \vec{P}_0 + s(\vec{P}_1 - \vec{P}_0) = \vec{P}_0 + s\vec{u} \tag{2.1}$$

$$\vec{Q}(t) = \vec{Q}_0 + t(\vec{Q}_1 - \vec{Q}_0) = \vec{Q}_0 + t\vec{v} \tag{2.2}$$

where, $\vec{u}$ and $\vec{v}$ are line direction vectors. Let a vector between the points on these two lines be given as

$$\vec{W}(s,t) = \vec{P}(s) - \vec{Q}(t) \tag{2.3}$$

For any n-dimensional space, the two lines L_1 and L_2 are closest at points $P_C = P(s_C)$ and $Q_C = Q(t_C)$ for which $W(s_C, t_C)$ is the global minimum for $W(s, t)$. If the two lines L_1 and L_2 are not parallel and do not intersect each other, then the segment $P_C Q_C$ joining these points is uniquely simultaneously perpendicular to
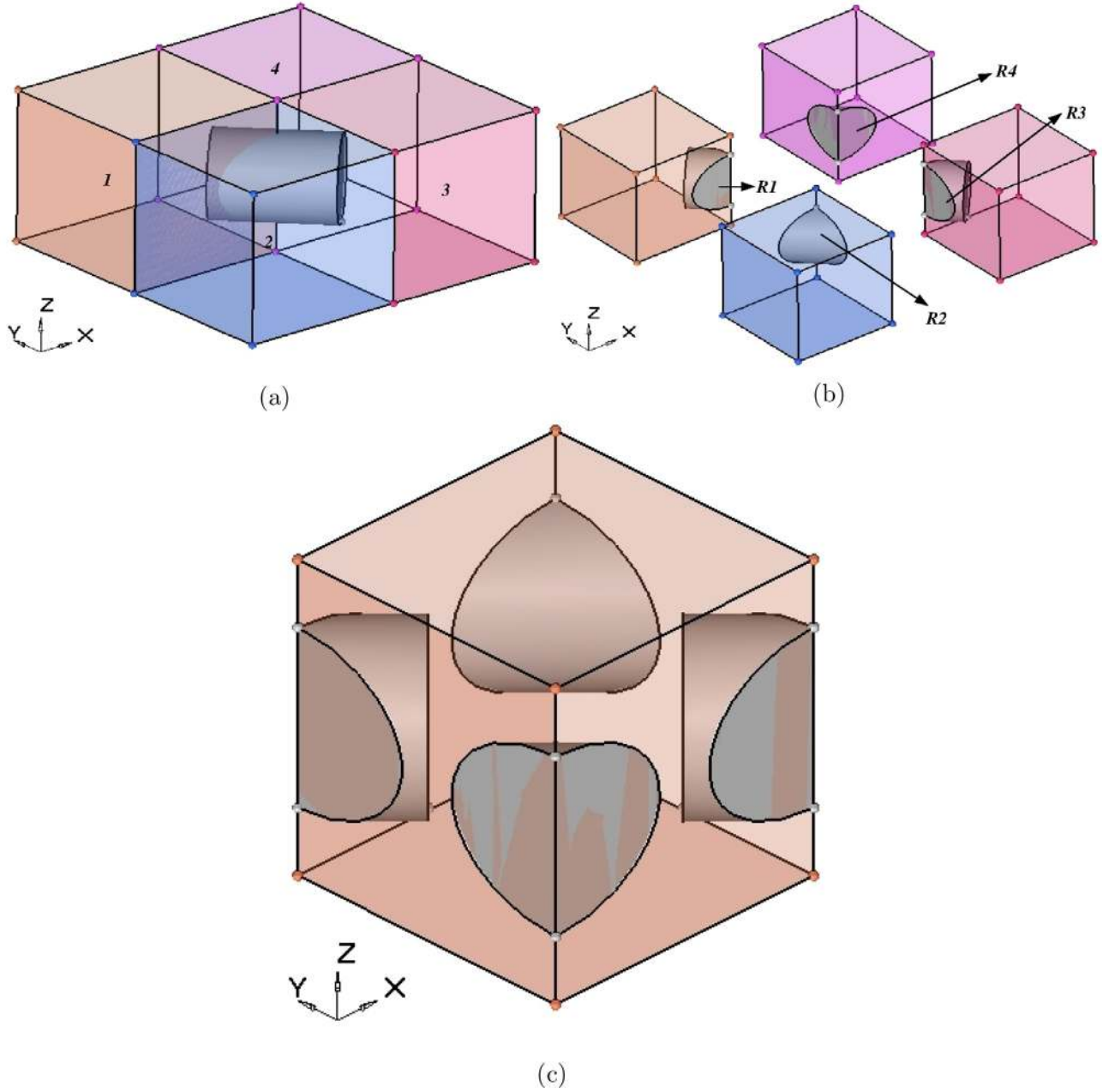
Fig. 5. Periodic fibres across an edge. (a) Fibre across an edge of a unit cell, (b) trimmed fibre across an edge, (c) RVE made with periodicity across an edge.

both lines. $\vec{W}_C = W(s_C, t_C)$ is uniquely perpendicular to line direction vectors $\vec{u}$ and $\vec{v}$ and this is equivalent to it by satisfying the following two conditions:

$$\vec{u} \cdot \vec{W}_C = 0 \quad \text{and} \quad \vec{v} \cdot \vec{W}_C = 0 \tag{2.4}$$

where, $\vec{W}_C = \vec{P}(s_C) - \vec{Q}(t_C) = \vec{W}_0 + s_C\vec{u} - t_C\vec{v}$. Now, substitute $\vec{W}_C$ in Eq. (2.4) and solving, we get

$$(\vec{u} \cdot \vec{u})s_c - (\vec{u} \cdot \vec{v})t_c = -\vec{u} \cdot \vec{W}_0 \tag{2.5}$$

$$(\vec{v} \cdot \vec{u})s_c - (\vec{v} \cdot \vec{v})t_c = -\vec{v} \cdot \vec{W}_0 \tag{2.6}$$

where, $\vec{W}_0 = \vec{P}_0 - \vec{Q}_0$. Let $a = \vec{u} \cdot \vec{u}$; $b = \vec{u} \cdot \vec{v}$; $c = \vec{v} \cdot \vec{v}$; $d = \vec{u} \cdot \vec{W}_0$ and $e = \vec{v} \cdot \vec{W}_0$. Substituting these values in Eq. (2.5) and Eq. (2.6) and

solving for s_C and t_C results in

$$s_C = \frac{be - cd}{ac - b^2} \quad \forall \ ac - b^2 \neq 0$$

$$t_C = \frac{ae - bd}{ac - b^2} \quad \forall \ ac - b^2 \neq 0 \tag{2.7}$$

If $ac - b^2 = 0$, it indicates that two lines are parallel and the distance between the lines is constant. This condition can be solved for parallel distance separation by constraining the value of one parameter and using either of the Eq. (2.7) to solve for the other as given below.

Now, let us select $s_C = 0$ and $t_C = \frac{d}{b} = \frac{e}{c}$. Substituting s_C and t_C instead of s and t in Eq. (2.1) and Eq. (2.2) indicating two points P_C and Q_C between two lines L_1 and L_2 where they are closest to
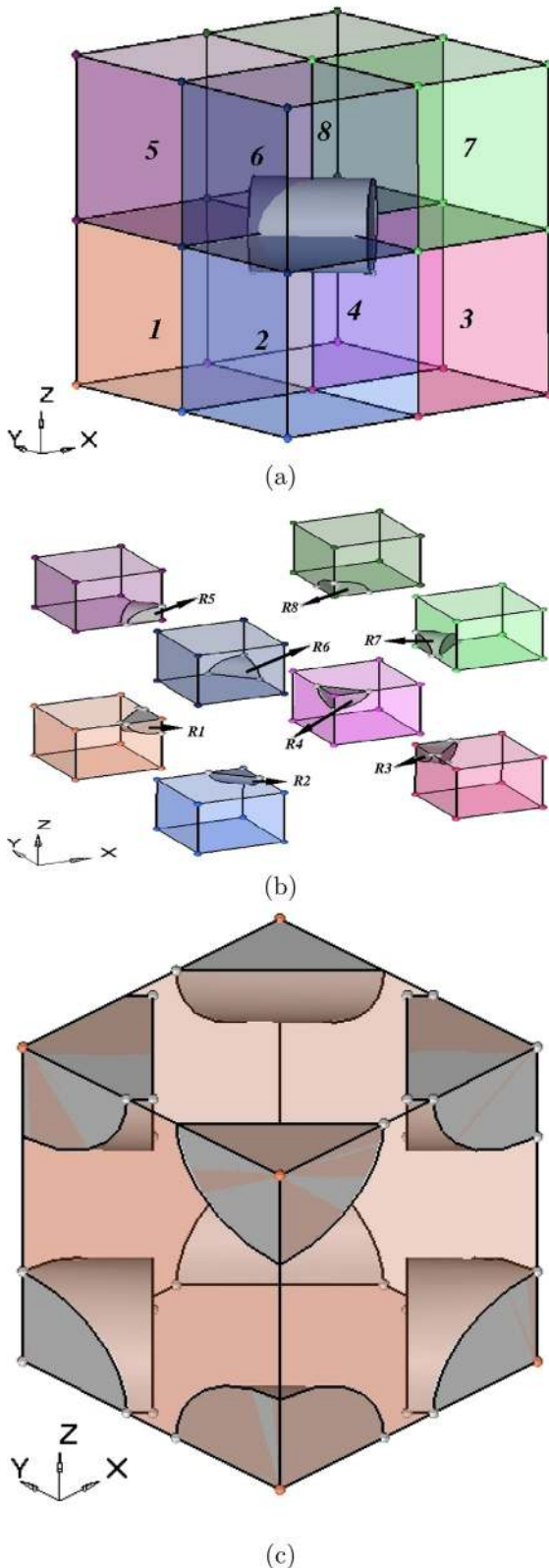
(a)

(b)

(c)

Fig. 6. Periodic fibres across a corner. (a) Fibre across a corner of a unit cell, (b) trimmed fibre across a corner, (c) RVE made with periodicity across a corner.
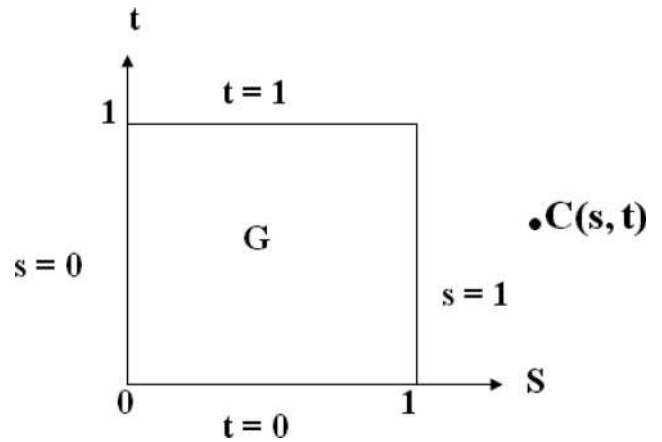

Fig. 7. A unit square in (s, t)-plane.

each other. The distance between them is given by

$$d(L_1, L_2) = \left| \vec{P}(s_C) - \vec{Q}(t_C) \right| = \left| (\vec{P}_0 - \vec{Q}_0) + \frac{(be - cd)\vec{u} - (ae - bd)\vec{v}}{ac - b^2} \right|$$

(2.8)

The distance measured by using Eq. (2.8) may not be the closest distance between two line segments due to its infiniteness. The segments on these lines are given as, respectively

Segment $S_1 = \vec{P}(S) = \vec{P}_0 + s(\vec{P}_1 - \vec{P}_0) = \vec{P}_0 + s\vec{u} \;\; \forall \; 0 \le s \le 1$

(2.9)

Segment $S_2 = \vec{Q}(S) = \vec{Q}_0 + t(\vec{Q}_1 - \vec{Q}_0) = \vec{Q}_0 + t\vec{v} \;\; \forall \; 0 \le t \le 1$

(2.10)

The first step in calculating distance between two segments is to get the closest points for infinite lines that they lie on. Hence, s_C and t_C for L_1 and L_2 are computed initially and if these are in the range of respective segments then they are the closest point. However, if they lie outside the range of either, then new points have to be determined that minimize $\vec{W}(s, t) = \vec{P}(s) - \vec{Q}(t)$ over the range of interest. So, quadratic minimization method has been implemented to determine the minimum length of W as it is same as minimizing length of $|W|^2$. Here, $|W|^2 = \vec{W} \cdot \vec{W} = (\vec{W}_0 + s\vec{u} - t\vec{v}) \cdot (\vec{W}_0 + s\vec{u} - t\vec{v})$, which is a quadratic function of s and t and defines a paraboloid over the (s, t)-plane with a minimum at $C = (s_C, t_C)$ (see Fig. 7), which is strictly increasing along the rays in the (s, t)-plane that start from C and go in any direction. But when segments are involved we need the minimum over a subregion G of the (s, t)-plane, and the global absolute minimum at C may lie outside the region G (see Fig. 7). However, in these cases the minimum always occurs on the boundary of G and in particular on the part of G's boundary that is visible to C, indicating a line from C to the boundary point which is exterior to G. It forms a unit square in this case. The four edges of the square are given by $s = 0, s = 1, t = 0, t = 1$ as shown in Fig. 7 and if $C = (s_C, t_C)$ is outside G then it can see at most two edges of G.

The conditions upon which the values s and t of the closest point between two line segments can be obtained, are as follows:

- If $s_C < 0$, C can see edge $s = 0$; If $s_C > 0$, C can see edge $s = 1$;
- If $t_C < 0$, C can see edge $t = 0$; If $t_C > 0$, C can see edge $t = 1$

Clearly, if C is not in G, then at least 1 or at most 2 of these inequalities are true, and they determine which edges of G are candidates for a minimum of $|W|^2$.

The procedure for the minimization for each candidate edge and basic calculus implemented to compute the minimum on that

Table 1
Fibre orientations in RVEs studied.

Cases	In Plane Orientation, $\phi°$	Out of Plane Orientation, $\theta°$
1	0	0
2	0-360	0
3	0-360	± 10
4	0-360	0-360

Table 2
Mechanical properties of AS4 carbon fibre material (Soden et al., 1998).

E_1 (GPa)	E_2 (GPa)	G_{12} (GPa)	G_{23} (GPa)	ν_{12}
225	15	15	7	0.2

Table 3
Mechanical properties of 3501-6 epoxy matrix material (Soden et al., 1998).

E (GPa)	G (GPa)	ν
4.2	1.567	0.35

edge, either in its interior or at an end point can be seen in the work of Schneider and Eberly (2002).

2.4. Computer implementation

RVE generation algorithm based on RSA technique has been implemented in MATLAB by modeling fibres as a line segment in a cube or cuboid. By using the information generated, a command file has been generated in MATLAB, which is imported in the commercial software HYPERMESH® to generate a solid RVE model maintaining periodicity in it. Since fibres get trimmed to maintain periodicity, the cross sectional shape of fibres may look elliptical. The tetrahedron elements are most suitable for such a geometry. Therefore, the tetrahedron elements are formed from a 2D triangular elements on the boundary. Initially, a solid RVE is meshed on one side of the surface of cube using 2D triangular elements and the same elements get duplicated and transformed to opposite face to maintain the periodicity. Similarly, elements for fibre on the surface get duplicated and transformed to the opposite face. To form a 3D tetrahedron mesh, elements formed through triangular mesh should be closed. To ensure closed volume, equivalence check is done. 3D tetrahedron matrix and fibre elements are created, which now represent an RVE with finite elements. Once the mesh has been generated using the required volume fraction, the software provides the coordinates and connectivity matrix for all the nodes generated. This data serves as an input for the finite element code for homogenization theory. A conjugate gradient solver is developed to solve the resulting system of equations.

The results obtained from the finite element implementation of homogenization theory for the prediction of effective properties from the RVEs generated are compared with those obtained from Halpin–Tsai (Halpin and Kardos, 1976) and Mori–Tanaka methods (Mori and Tanaka, 1973; Mura, 1987). The details of these methods are presented in Appendix A. The finite element and the periodic boundary conditions implementation is presented in Appendix B.

3. Results and discussion

In this section, effects of fibre orientation and fibre volume fraction on the effective properties of RVE developed using RSA algorithm and the material behaviour based on fibre orientation are discussed.

To study the effect of orientation of fibre in chopped fibre reinforced composites, four different types of RVEs have been developed. Firstly, RVEs have been developed with all chopped fibres aligned in a particular direction. Secondly, all the fibres were randomly oriented in on of the plane (here *XY*-plane is chosen) and restricted in remaining planes of an RVE generated. Next, RVE is created with randomly oriented fibres in one plane (*XY*-plane) and partially oriented in another plane (here *XZ*-plane is chosen). The orientation restricted to another plane is $\pm 10°$. Finally, an RVE with completely random oriented fibres in all planes is generated. Table 1 represents the summarised form of different cases considered in this study for the effect of fibre orientation on effective properties. The material considered in this study is AS4 carbon fibre and 3501-6 Epoxy matrix (Soden et al., 1998). The material

properties of the fibre and matrix materials are given in Table 2 and Table 3, respectively.

To generate random distribution in an RVE, uniform distribution function (available in MATLAB) had been used in RSA algorithm. RVEs are generated for different volume fractions for all the cases mentioned in Table 1. For a given volume fraction 5 RVEs are generated to see the efficacy of methodology adopted to generate RVE in repeating the predicted effective stiffness. The fibres considered in this study are of cylindrical in shape. Initially, fibres are generated with its center at origin aligned along *X* direction and then translated to randomly generated coordinates inside the RVE by using uniform distribution function with geometric periodicity until a desired volume fraction is achieved. The dimensions of RVE are chosen based on previous study carried out by Iorga et al. (2008) as $2l_f \times 2l_f \times 4d_f$, where l_f is the length and d_f is the diameter of short fibres considered. In the current study the estimation of RVE size not emphasized, rather the approach used in Iorga et al. (2008) has been used to choose the RVE sizes. Further, the RVE size chosen above is for the case of completely random oriented fibre case. More details can be seen in Iorga et al. (2008) and references therein.

Once the RVE size is chosen the fibres are added sequentially as discussed earlier. This procedure of adding fibres to an RVE is continued till no more fibres can be added to it without touching the already added fibres in the RVE. Since, the size of the RVE and number of fibres are known the fibre volume fraction of the resulting material can be calculated. It should be noted that in maintaining the periodicity if any fibre is coming out of the RVE then that part is placed inside the RVE. Thus, the number of fibres in an RVE is always a whole number.

Remark 3. In the generation of RVE with the periodic condition only the integer number of fibres are added in it. Furthermore, the size of the RVE is kept fixed. Thus, depending upon the aspect ratio of the fibres and their orientations a certain volume fraction could be achieved like 15.43%, 21.03%, etc. but these same volume fractions could not be achieved for all the cases studied. However, to have a fair comparison, it has been tried to achieve almost the same volume fractions for all cases studied.

3.1. Case 1: in-plane aligned fibres

In this section effective properties of aligned fibre composites and its material behaviour is studied in detail. The convergence criterion for aligned fibre composite properties is also reviewed in detail.

In this case, fibres were not allowed to orient in any direction during the generation of RVEs. Four different fibre volume fractions of 15.43%, 18.23%, 21.03%, 22.44% are considered to study the effective material properties and their behaviour. The maximum volume fraction which can be achieved using RSA algorithm for this case
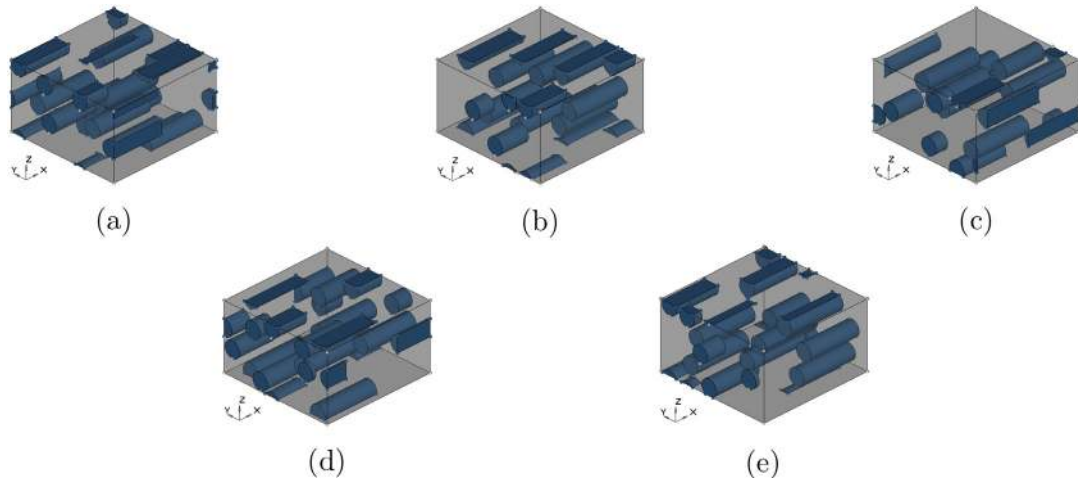
Fig. 8. RVEs for Case 1 with fibre volume fraction of 15.43%. (a) RVE 1, (b) RVE 2, (c) RVE 3, (d) RVE 4, (e) RVE 5.
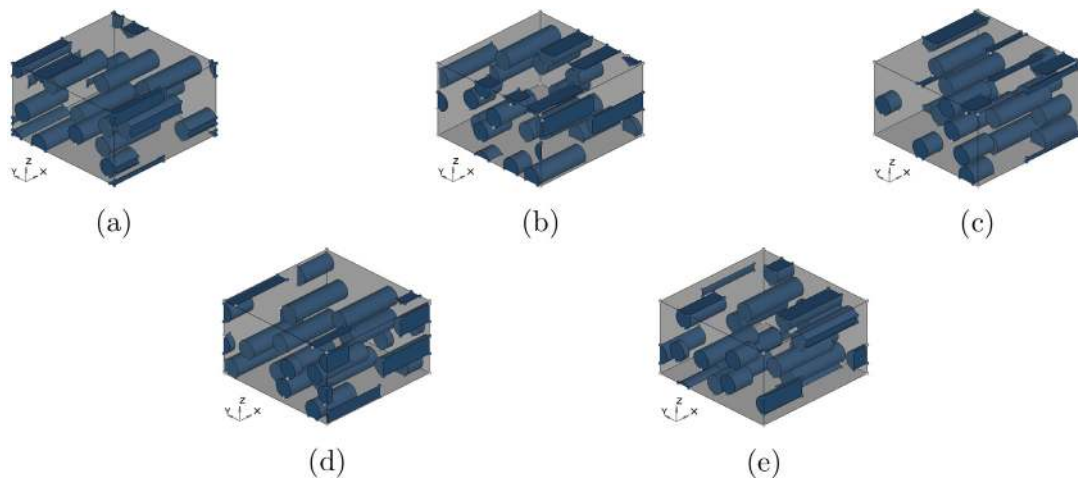
Fig. 9. RVEs for Case 1 with fibre volume fraction of 18.43%. (a) RVE 1, (b) RVE 2, (c) RVE 3, (d) RVE 4, (e) RVE 5.
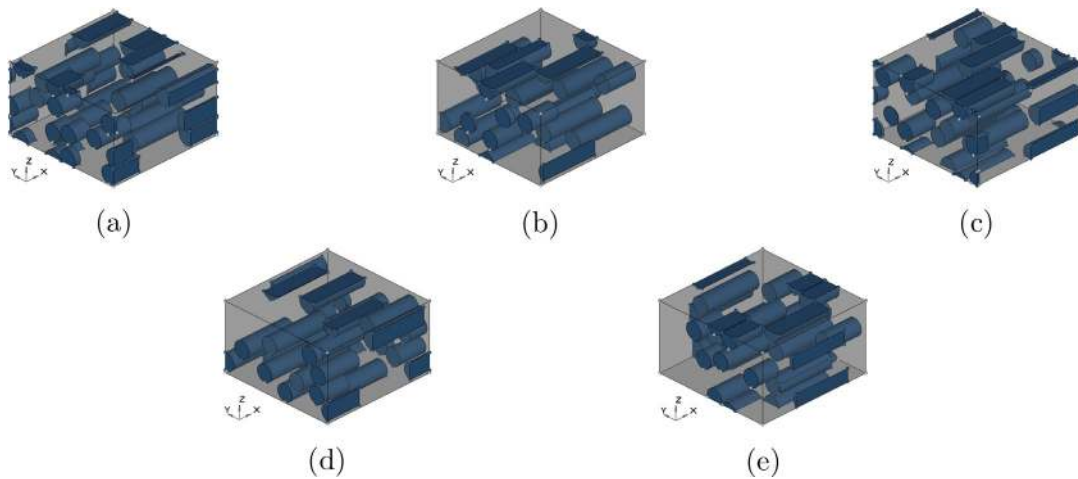
Fig. 10. RVEs for Case 1 with fibre volume fraction of 21.03%. (a) RVE 1, (b) RVE 2, (c) RVE 3, (d) RVE 4, (e) RVE 5.

is 22.44% with 16 cylinders of aspect ratio 3.5. Five models of RVE for each volume fraction have been generated as shown in Figs. 8, 9, 10 and 11, respectively. Fig. 12 shows a typical meshed RVE used in the analysis. One can note that the exact meshes are reproduced on opposite faces of the RVE to ensure periodic boundary conditions.

The effective stiffness tensors obtained by analyzing the RVEs for fibre volume fraction of 15.43 and 22.44% are given in Tables 4 and 5, respectively as examples. The subscripts used with these tensors denote the corresponding RVE. It is to be noted that all these tensors are symmetric.

Table 4
Effective stiffness tensors for all fibres aligned case with fibre volume fraction of 15.43% (Values in MPa).

$$[C]_1 = \begin{bmatrix} 11886 & 3500 & 3504 & 0 & 0 & 85 \\ & 7170 & 3328 & 0 & 4 & 5 \\ & & 7176 & 0 & 0 & 0 \\ & & & 1907 & 0 & 0 \\ & & & & 2130 & 0 \\ & & & & & 2112 \end{bmatrix}, \quad [C]_2 = \begin{bmatrix} 11650 & 3482 & 3480 & 0 & 5 & 0 \\ & 7164 & 3343 & 0 & 0 & 0 \\ & & 7162 & 2 & 0 & 7 \\ & & & 1931 & 0 & 2 \\ & & & & 2095 & 0 \\ & & & & & 2097 \end{bmatrix},$$

$$[C]_3 = \begin{bmatrix} 12396 & 3532 & 3485 & 0 & 37 & 0 \\ & 7166 & 3337 & 2 & 0 & 5 \\ & & 7164 & 0 & 5 & 0 \\ & & & 1909 & 0 & 0 \\ & & & & 2108 & 0 \\ & & & & & 2139 \end{bmatrix}, \quad [C]_4 = \begin{bmatrix} 11386 & 3450 & 3560 & 10 & 98 & 5 \\ & 7168 & 3347 & 0 & 3 & 0 \\ & & 7153 & 18 & 3 & 4 \\ & & & 1918 & 3 & 13 \\ & & & & 2121 & 22 \\ & & & & & 2091 \end{bmatrix},$$

$$[C]_5 = \begin{bmatrix} 11374 & 3537 & 3477 & 10 & 84 & 2 \\ & 7146 & 3340 & 0 & 1 & 8 \\ & & 7195 & 0 & 7 & 0 \\ & & & 1906 & 0 & 9 \\ & & & & 2135 & 0 \\ & & & & & 2082 \end{bmatrix}$$

Table 5
Effective stiffness tensors for all fibres aligned case with fibre volume fraction of 22.44% (Values in MPa).

$$[C]_1 = \begin{bmatrix} 14002 & 3535 & 3568 & 0 & 45 & 14 \\ & 7563 & 3303 & 11 & 0 & 0 \\ & & 7559 & 0 & 6 & 0 \\ & & & 2129 & 0 & 1 \\ & & & & 2432 & 0 \\ & & & & & 2412 \end{bmatrix}, \quad [C]_2 = \begin{bmatrix} 14694 & 3607 & 3558 & 12 & 69 & 0 \\ & 7562 & 3308 & 0 & 0 & 0 \\ & & 7539 & 1 & 4 & 2 \\ & & & 2112 & 0 & 3 \\ & & & & 2407 & 0 \\ & & & & & 2487 \end{bmatrix},$$

$$[C]_3 = \begin{bmatrix} 13900 & 3638 & 3548 & 0 & 104 & 0 \\ & 7545 & 3305 & 14 & 0 & 0 \\ & & 7574 & 3 & 9 & 3 \\ & & & 2091 & 0 & 11 \\ & & & & 2434 & 14 \\ & & & & & 2435 \end{bmatrix}, \quad [C]_4 = \begin{bmatrix} 14514 & 3599 & 3559 & 5 & 0 & 0 \\ & 7539 & 3322 & 12 & 0 & 12 \\ & & 7537 & 0 & 4 & 0 \\ & & & 2129 & 0 & 0 \\ & & & & 2425 & 14 \\ & & & & & 2471 \end{bmatrix},$$

$$[C]_5 = \begin{bmatrix} 14303 & 3619 & 3564 & 0 & 0 & 0 \\ & 7521 & 3322 & 0 & 8 & 0 \\ & & 7558 & 9 & 0 & 10 \\ & & & 2107 & 9 & 5 \\ & & & & 2461 & 16 \\ & & & & & 2425 \end{bmatrix}$$

Table 6
Properties of aligned short fibre composites: Case 1.

| V_f (%)	RVE No.	E_1 (GPa)	E_2 (GPa)	E_3 (GPa)	G_{12} (GPa)	G_{13} (GPa)	G_{23} (GPa)	ν_{12}	ν_{13}	ν_{23}	a_{YZ}	a
	1	9.548	5.280	5.284	2.111	2.130	1.907	0.333	0.334	0.374	0.992	0.774
	2	9.344	5.258	5.256	2.097	2.095	1.931	0.331	0.331	0.376	1.011	0.782
15.43	3	10.051	5.271	5.293	2.140	2.109	1.909	0.340	0.328	0.379	0.997	0.752
	4	9.042	5.271	5.199	2.091	2.120	1.918	0.319	0.349	0.376	1.006	0.798
	5	9.029	5.214	5.288	2.082	2.135	1.906	0.344	0.324	0.368	0.996	0.797
	HT	10.061	5.403	5.403	2.019	2.019	1.845	0.321	0.321	0.29	-	-
	MT	8.596	5.683	5.683	2.190	2.190	2.04	0.338	0.338	0.383	-	-
	1	10.558	5.482	5.486	2.219	2.230	1.988	0.331	0.331	0.371	0.994	0.749
	2	9.969	5.401	5.416	2.244	2.198	1.996	0.338	0.327	0.372	1.013	0.782
18.43	3	10.982	5.467	5.502	2.208	2.253	1.998	0.334	0.326	0.375	1.002	0.735
	4	11.246	5.471	5.511	2.222	2.229	1.980	0.339	0.324	0.375	0.993	0.721
	5	10.454	5.426	5.517	2.216	2.242	1.975	0.347	0.317	0.368	0.989	0.756
	HT	11.338	5.642	5.642	2.118	2.118	1.890	0.311	0.311	0.302	-	-
	MT	9.643	6.019	6.019	2.339	2.339	2.170	0.338	0.338	0.387	-	-
	1	11.142	5.654	5.783	2.354	2.348	2.073	0.352	0.304	0.356	0.985	0.748
	2	11.569	5.696	5.700	2.345	2.368	2.055	0.330	0.331	0.364	0.984	0.733
21.03	3	11.538	5.622	5.694	2.410	2.361	2.081	0.347	0.315	0.366	1.006	0.746
	4	11.750	5.698	5.668	2.371	2.399	2.063	0.323	0.339	0.368	0.992	0.735
	5	11.983	5.612	5.673	2.402	2.318	2.075	0.346	0.314	0.372	1.011	0.724
	HT	12.741	5.903	5.903	2.212	2.212	1.948	0.311	0.311	0.278	-	-
	MT	10.616	6.328	6.328	2.477	2.477	2.277	0.338	0.338	0.389	-	-
	1	11.679	5.802	5.785	2.418	2.432	2.129	0.323	0.331	0.361	1.000	0.746
	2	12.327	5.788	5.789	2.487	2.407	2.112	0.335	0.325	0.365	0.996	0.725
22.44	3	11.518	5.746	5.811	2.435	2.433	2.091	0.342	0.319	0.356	0.983	0.752
	4	12.156	5.754	5.769	2.471	2.425	2.129	0.334	0.325	0.366	1.010	0.735
	5	11.927	5.727	5.783	2.425	2.462	2.107	0.339	0.323	0.363	0.999	0.741
	HT	13.448	6.024	6.024	2.257	2.257	2.091	0.313	0.313	0.281	-	-
	MT	11.171	6.504	6.504	2.556	2.556	2.339	0.338	0.338	0.390	-	-
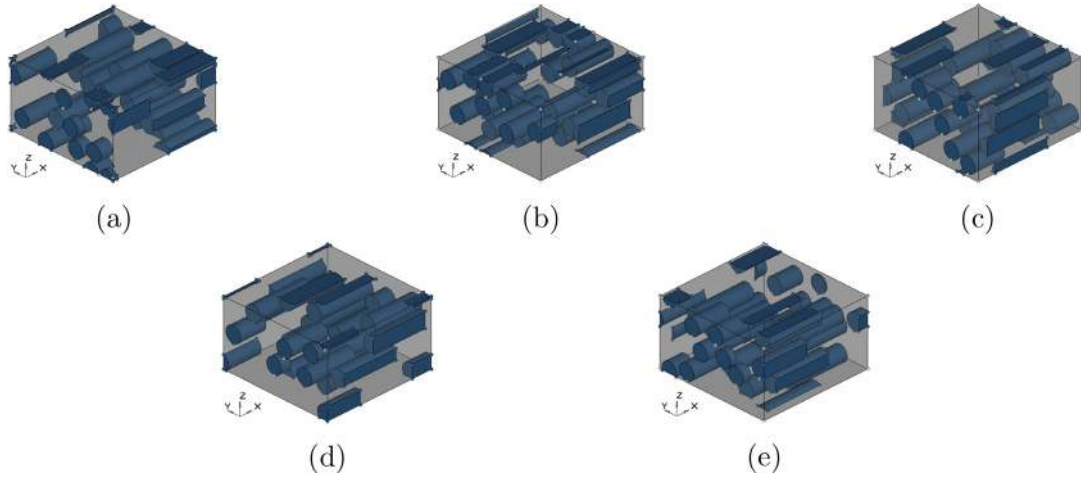
Fig. 11. RVEs for Case 1 with fibre volume fraction of 22.44%. (a) RVE 1, (b) RVE 2, (c) RVE 3, (d) RVE 4, (e) RVE 5.
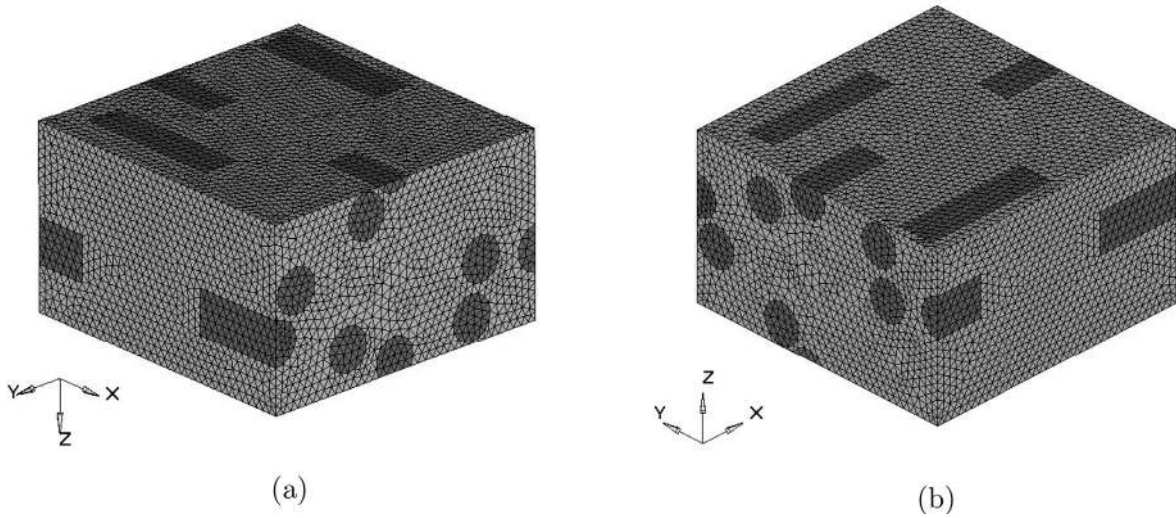

Fig. 12. A typical meshed RVE for Case 1. (a) meshes on positive *x, y* and negative *z* faces, (b) meshes on negative *x, y* and positive *z* face.

Remark 4. Note that the *X, Y* and *Z* directions are represented as 1, 2 and 3, respectively. Further, the stress and strain vectors, for the resulting constitutive material, are arranged as $\{\sigma_{11}\,\sigma_{22}\,\sigma_{33}\,\sigma_{23}\,\sigma_{13}\,\sigma_{12}\}^T$ and $\{\varepsilon_{11}\,\varepsilon_{22}\,\varepsilon_{33}\,\varepsilon_{23}\,\varepsilon_{13}\,\varepsilon_{12}\}^T$, respectively. The components of effective stiffness tensor C_{ij} have one to one correspondence with respect to these vectors.

To quantify the closeness of in-plane isotropic behaviour of an RVE with fibres aligned in *XY*-plane, a parameter based on stiffness tensor entries relation for transversely isotropic behaviour is defined as

$$a_{YZ} = \frac{2C_{44}}{C_{22}^{yz} - C_{23}} \qquad (3.1)$$

where, $C_{22}^{yz} = \frac{C_{22} + C_{33}}{2}$ and C_{ij} are the components of effective stiffness tensor. It is to be noted that the fibres are aligned along *X* direction. Therefore, it is expected for this case that the macroscopic behaviour will be isotropic in a plane perpendicular to *X*-axis, that is, the *YZ*-plane. However, one can define such a parameter for any other plane as well. Further, to check if the overall material behaviour is isotropic, a non dimensional parameter, *a* is employed here. This is defined based on the stiffness entries relation for a typical isotropic material behaviour as

$$a = \frac{2Y_{44}}{Y_{11} - Y_{12}} \qquad (3.2)$$

where, $Y_{11} = \frac{C_{11} + C_{22} + C_{33}}{3}$; $Y_{12} = \frac{C_{12} + C_{23} + C_{31}}{3}$ and $Y_{44} = \frac{C_{44} + C_{55} + C_{66}}{3}$. Thus, the parameter a_{YZ} is an indicator of in-plane isotropy for *YZ*-plane, whereas the parameter *a* is an indicator of overall isotropy. When the value of $a_{YZ} = 1$ then the material is isotropic in *YZ*-plane and when *a* approaches 1 the material is said to be isotropic. The relations between stiffness entries for various material behaviour can be seen from their stiffness tensor (for example see Mohite). Similar definitions of parameters are proposed in Kanit et al., (2006).

Substituting the entries from effective stiffness tensor obtained from homogenization model, a_{YZ} values are obtained and tabulated in Table 6. The mean and standard deviation in these values for all fibre volume fractions studied are reported in Table 7. Thus, from these tables it is seen that this material indicates more than 99% isotropic behaviour in *YZ*-plane, that is, macroscopic behaviour is transversely isotropic. The parameter *a* has the values above 0.72 as can be seen from Table 7. This indicates that macroscopic behaviour is not isotropic. Further, from this table it can also be seen that as the fibre volume fraction increases the mean value of the parameter *a* decreases. This can be explained on the basis of fibre packing geometry. Let us measure the contribution of the fibres towards stiffness of the resulting material in terms of their projected areas on the planes of an RVE. As can be seen from the RVEs shown in Figs. 8 through 11, the increase in projected area

Table 7
Average and SD for properties of Case 1.

Property	V_f 15.43 (%)		V_f 18.43 (%)		V_f 21.03 (%)		V_f 22.44 (%)	
	Mean	SD	Mean	SD	Mean	SD	Mean	SD
E_1 (GPa)	9.402	0.422	10.641	0.493	11.596	0.309	11.921	0.332
E_2 (GPa)	5.258	0.026	5.449	0.034	5.656	0.040	5.763	0.031
E_3 (GPa)	5.264	0.038	5.486	0.041	5.703	0.046	5.787	0.015
G_{12} (GPa)	2.104	0.022	2.221	0.013	2.376	0.028	2.447	0.030
G_{13} (GPa)	2.117	0.016	2.230	0.020	2.358	0.029	2.431	0.019
G_{23} (GPa)	1.914	0.010	1.987	0.009	2.069	0.010	2.113	0.016
ν_{12}	0.334	0.009	0.337	0.006	0.339	0.0012	0.334	0.007
ν_{13}	0.333	0.009	0.324	0.005	0.320	0.014	0.324	0.004
ν_{23}	0.374	0.004	0.372	0.003	0.365	0.006	0.362	0.003
a_{YZ}	1.000	0.008	0.998	0.009	0.996	0.012	0.997	0.009
a	0.781	0.019	0.748	0.023	0.737	0.009	0.739	0.011

Table 8
Percentage difference in properties by homogenization theory with respect to Mori–Tanaka and Halpin–Tsai model.

Property	V_f 15.43 (%)		V_f 18.43 (%)		V_f 21.03 (%)		V_f 22.44 (%)	
	MT	HT	MT	HT	MT	HT	MT	HT
E_1	8.96	6.81	10.59	6.51	8.82	9.38	6.50	12.17
E_2	7.76	2.60	9.56	3.43	11.22	4.06	12.07	4.36
E_3	7.65	2.50	8.88	2.76	10.39	3.22	11.66	3.94
G_{12}	4.03	4.32	4.73	5.11	4.17	7.18	4.35	7.76
G_{13}	3.39	4.96	4.34	5.51	4.92	6.44	5.00	7.13
G_{23}	7.04	3.92	8.42	4.66	9.59	5.66	10.12	6.25
ν_{12}	1.55	4.63	0.15	7.75	0.44	9.15	1.01	8.12
ν_{13}	1.64	4.54	4.04	3.86	5.34	3.36	4.08	5.06
ν_{23}	2.35	22.61	3.9	24.47	6.39	25.22	7.49	25.74

on YZ plane as compared to other planes is lesser. Furthermore, as the fibre volume fraction increases the projected areas on the three planes are not increased proportionately. Thus, the stiffness contribution due to fibre volume fraction increase is more in other planes as compared to that for YZ plane. This can be clearly seen from Tables 4 and 5 as well. Thus, the parameter a shows a small decrement in its value as the fibre volume fraction is increased.

The effective engineering properties/constants are deduced from the coefficients obtained by inverting these tensors (compliance tensors). The effective properties obtained from homogenization technique for all the five RVE models for all volume fraction are reported in Table 6. The obtained results are compared with those of Mori–Tanaka (denoted by MT) and Halpin–Tsai (denoted by HT) methods.

From these results it can be seen that for all the fibre volume fractions studied the results of the homogenization method lie between Mori–Tanaka and Halpin–Tsai methods. Further, it can be seen that as the volume fraction increases, the Young's moduli and shear moduli increase and the Poisson's ratios decrease slightly. This is because at low volume fractions RVE is almost filled with low stiffness epoxy material and as fibre volume fraction increases matrix content reduces and fibre starts withstanding load, which is comparatively a stiffer material leading to decrease in Poisson's effect. Since fibres are aligned in X direction, effective elastic constants like Young's moduli and shear moduli are high in that direction compared to other directions.

The mean values of the effective properties for the RVEs for their respective fibre volume fractions along with standard deviation (SD) for these values are reported in Table 7. The percentage standard deviation among the properties is comparatively higher for E_1 values and close to zero for the remaining properties. It can be seen from Table 7 that as the volume fraction increases, SD for E_1 decreases slightly and there seems no change for remaining properties. The variation in effective properties among different RVE models of a volume fraction is due to random packing and periodic arrangements of fibres in that RVE.

Table 8 indicates the percentage difference between mean values of effective properties obtained from homogenization model implemented with respect to Mori–Tanaka and Halpin–Tsai models. It is seen that this percentage difference is less for Halpin–Tsai method than Mori–Tanaka method in the respective properties, except the out of plane Poisson's ratio in transverse direction, ν_{23}. It is further seen that, in general, as the volume fraction increases this difference increases for both methods. For Young's moduli this difference varies between 2.5% to 12%, for shear moduli it is between 3% to 10% and for Poisson's ratio the maximum difference is seen upto 26%. This maximum difference is seen with respect to Halpin–Tsai method for ν_{23}. Furthermore, this maximum difference is because the fibre packing fraction is not considered in Halpin–Tsai model. Also, the engineering constants of short fibre

composite are weakly dependent on fibre aspect ratio and hence approximated using continuous fibre formulae.

Remark 5. The values of the engineering constants reported for the effective behaviour in Table 9 assumes that the degree of anisotropy for the effective stiffness tensors is negligibly small. For example, the highest upper right 3×3 non-zero entry for $[C]_1$ when compared with the smallest upper left 3×3 entry is less than 3%. A similar observation is made in the studies carried out by Kanit et al. (2006) and Iorga et al. (2008). Therefore, the effective stiffness tensor is assumed to have the coefficients corresponding to normal-normal coupling part (upper left 3×3 entries) and diagonal entries for shear part only (diagonal entries of lower right 3×3 entries) and all other entries are made zero. Then this is inverted to evaluate the engineering constants. When the engineering constants obtained from this approach are compared with those obtained by retaining all the terms in original effective stiffness tensor of an RVE (as given in Tables 4 and 5) then no significant change in the values is observed. The values shown in boxes in Table 9 are the values with a negligible change when compared to those in Table 6. The maximum change is less than 1%. Thus, this also shows that the degree of anisotropy is not significant. Therefore, for the remaining cases studied in the following, this anisotropy is not ignored while calculating the properties of RVEs.

A brief convergence study is also carried out for finite element computations by investigating the numerical results as the numbers of elements are increased in the domain (RVE). A set of numerical solutions for in-plane aligned fibres case has been made for five different meshes based on the number of elements used in these meshes. Here, the convergence of engineering constants E_1, E_2, G_{12}, G_{23}, ν_{12} and ν_{23} is studied. The number of elements are varied from 5×10^4 to 3×10^5. The results obtained for various mesh sizes interpret that around 2×10^5 number of elements the results (that is, property values) are converged. Hence, for the remaining models of RVE, mesh size with number of elements 2×10^5 and above are used to discretize the model. The linear tetrahedron elements are used to obtain the solution. The convergence of the engineering constants with the number of elements is shown in Fig. 13.

3.2. Case 2: In-plane randomly oriented fibres

In this section, the material behaviour of RVEs generated with random in-plane orientation of fibres in XY-plane is studied in detail. In the RVEs generated, initially the fibres with their centres located at different positions, are aligned along X-axis. The location of centres of these fibres are generated randomly with a uniform probability distribution function. Then these fibres are oriented randomly about Z-axis, again with a uniform probability distribution function. The fibres are allowed neither to intersect nor to overlap each other. RVEs with three different volume

Table 9
Properties of aligned short fibre composites: Case 1. Properties obtained ignoring anisotropy completely. Boxes show changed values as compared to given in Table 6.

| V_f (%)	RVE No.	E_1 (GPa)	E_2 (GPa)	E_3 (GPa)	G_{12} (GPa)	G_{13} (GPa)	G_{23} (GPa)	ν_{12}	ν_{13}	ν_{23}
15.43	1	9.551	5.280	5.284	2.112	2.130	1.907	0.333	0.334	0.374
	2	9.344	5.258	5.256	2.097	2.095	1.931	0.331	0.331	0.376
	3	10.051	5.271	5.293	2.139	2.109	1.909	0.340	0.328	0.379
	4	9.042	5.271	5.199	2.091	2.121	1.918	0.318	0.348	0.375
	5	9.032	5.214	5.287	2.082	2.136	1.906	0.343	0.324	0.368
18.43	1	10.558	5.482	5.486	2.219	2.230	1.988	0.331	0.331	0.371
	2	9.969	5.401	5.416	2.244	2.198	1.996	0.338	0.327	0.372
	3	10.982	5.467	5.502	2.208	2.253	1.998	0.334	0.326	0.375
	4	11.247	5.471	5.511	2.222	2.229	1.980	0.339	0.324	0.375
	5	10.467	5.426	5.517	2.218	2.242	1.975	0.347	0.317	0.368
21.03	1	11.148	5.654	5.783	2.354	2.348	2.073	0.352	0.304	0.356
	2	11.569	5.696	5.700	2.345	2.368	2.055	0.330	0.331	0.364
	3	11.538	5.622	5.694	2.410	2.361	2.081	0.347	0.315	0.366
	4	11.750	5.698	5.668	2.371	2.399	2.063	0.323	0.339	0.368
	5	11.983	5.612	5.673	2.402	2.318	2.075	0.346	0.314	0.372
22.44	1	11.680	5.802	5.785	2.418	2.432	2.129	0.323	0.331	0.361
	2	12.327	5.788	5.789	2.487	2.407	2.112	0.335	0.325	0.365
	3	11.522	5.746	5.811	2.435	2.434	2.091	0.342	0.319	0.356
	4	12.156	5.754	5.769	2.471	2.425	2.129	0.334	0.325	0.366
	5	11.927	5.727	5.783	2.425	2.462	2.107	0.339	0.323	0.363
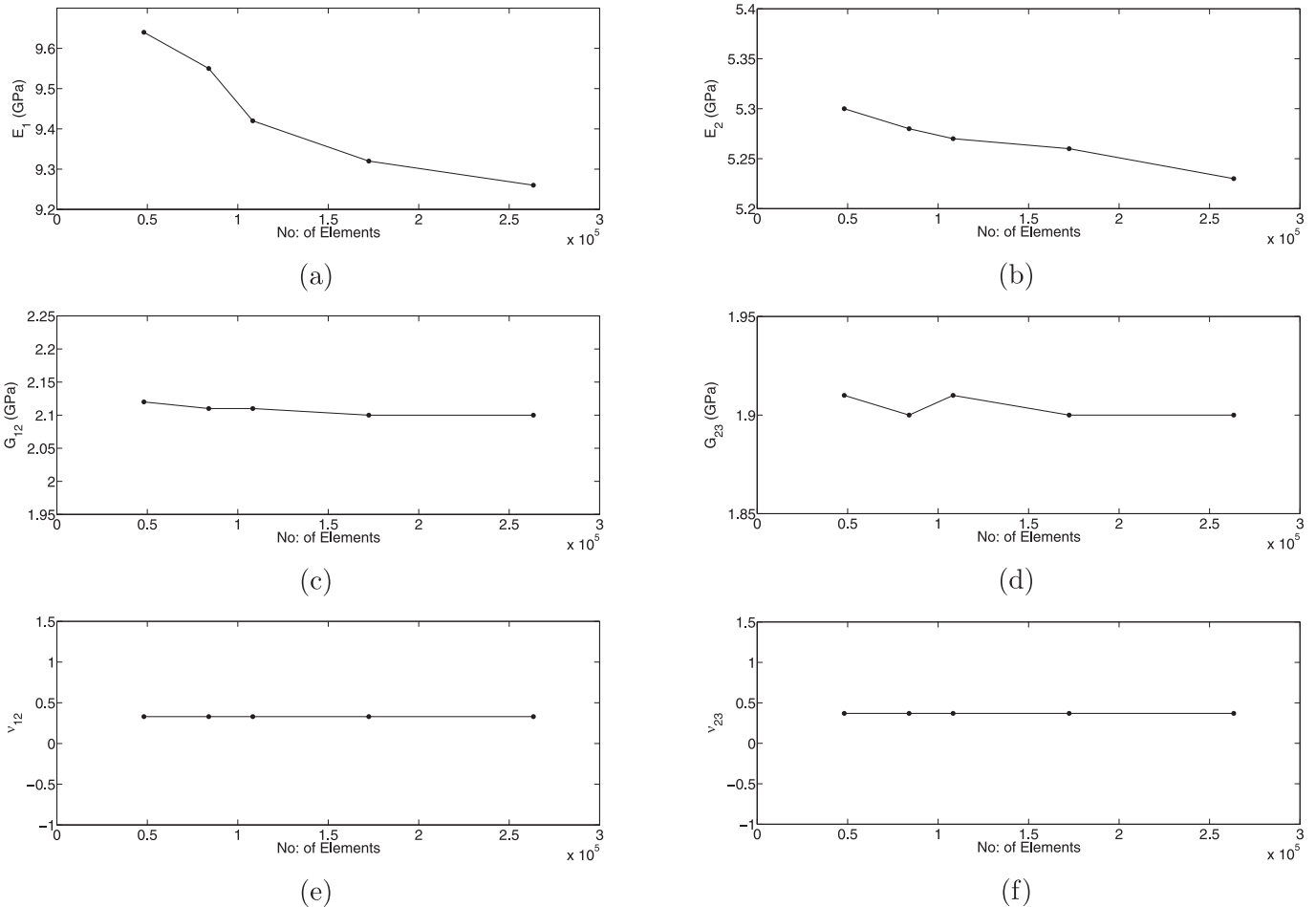
Fig. 13. Convergence of engineering constants with number of elements in an RVE for Case 1. (a) E_1, (b) E_2, (c) G_{12}, (d) G_{23}, (e) ν_{12}, (f) ν_{23}.
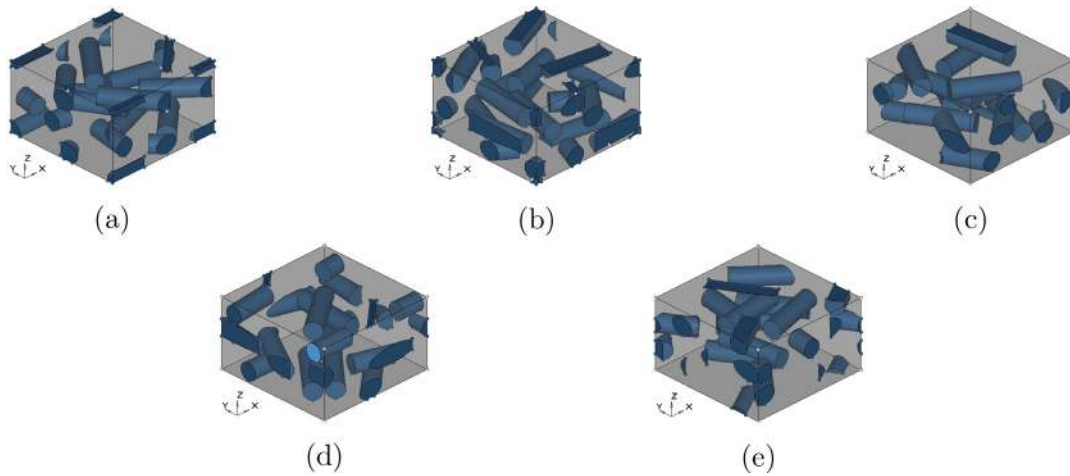
Fig. 14. RVEs for Case 2 with fibre volume fraction of 15.43%. (a) RVE 1, (b) RVE 2, (c) RVE 3, (d) RVE 4, (e) RVE 5.
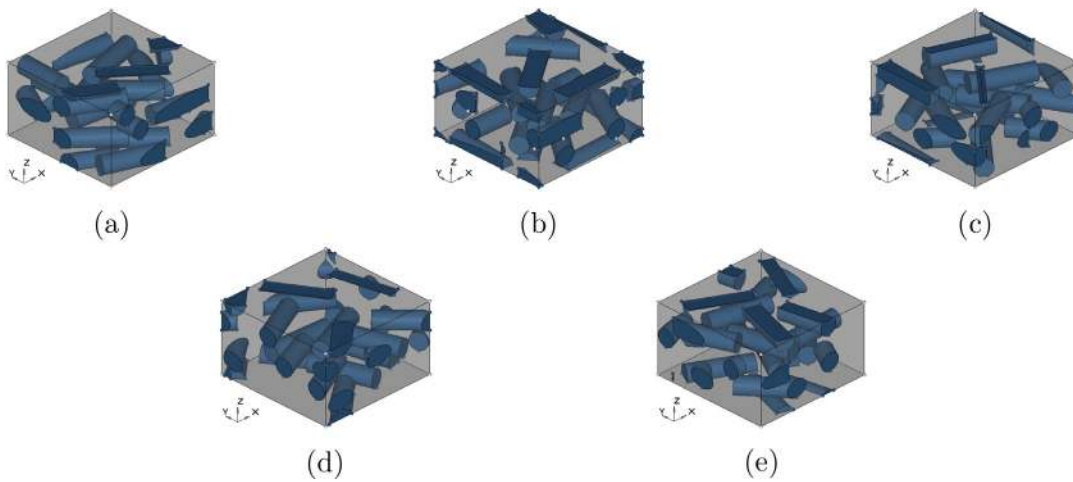

Fig. 15. RVEs for Case 2 with fibre volume fraction of 18.23%. (a) RVE 1, (b) RVE 2, (c) RVE 3, (d) RVE 4, (e) RVE 5.
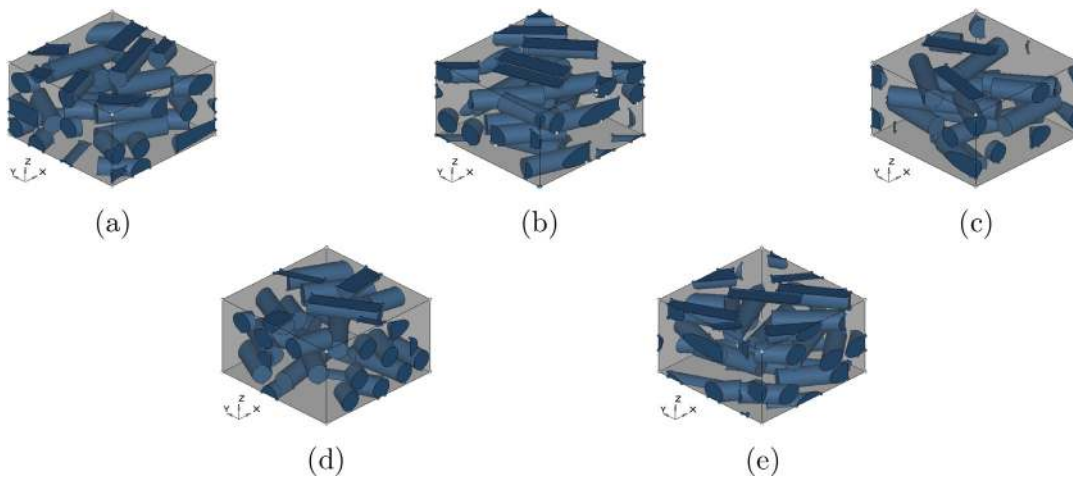

Fig. 16. RVEs for Case 2 with fibre volume fraction of 22.44%. (a) RVE 1, (b) RVE 2, (c) RVE 3, (d) RVE 4, (e) RVE 5.

fractions have been generated with a maximum volume fraction of 22.44%. Five different models of RVEs for volume fractions of 15.43%, 18.23% and 22.44% have been generated to study the effect of fibre volume fraction on the behaviour of RVEs. The RVEs for these volume fractions are shown in Figs. 14, 15 and 16, respectively. Fig. 17 shows an RVE with meshing used in the finite element analysis.

Table 10 represents the effective material properties obtained through homogenization technique for different volume fractions. It is observed that for a given volume fraction the Young's modulus in *X* and *Y* directions are close to each other compared to *Z* direction, whereas the values of shear moduli and Poisson's ratios are close to each other in out of plane directions (*XZ* and *YZ* plane). This is due the fact that fibres are having random orienta-
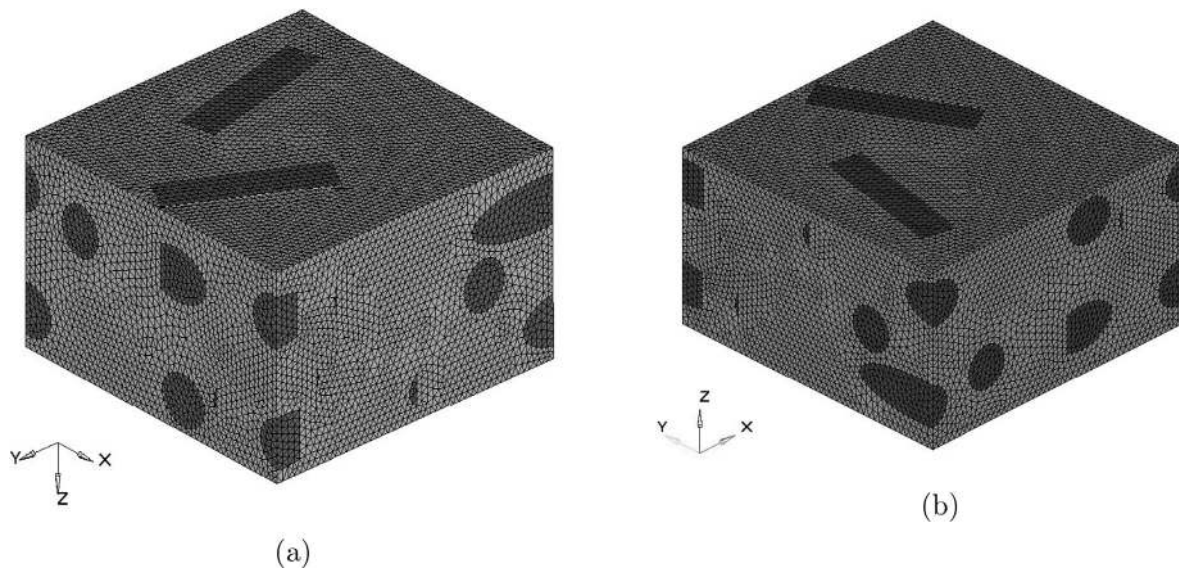
Fig. 17. A typical meshed RVE for Case 2. (a) Meshes on positive *x, y* and negative *z* faces, (b) meshes on negative *x, y* and positive *z* face.

Table 10
Properties of in-plane oriented short fibre composites: Case 2.

V_f (%)	Model	E_1 (GPa)	E_2 (GPa)	E_3 (GPa)	G_{12} (GPa)	G_{13} (GPa)	G_{23} (GPa)	v_{12}	v_{13}	v_{23}	a_{YZ}	a
15.43	1	6.774	6.337	5.425	2.783	2.021	2.005	0.356	0.306	0.314	0.873	0.952
	2	6.707	6.412	5.285	2.367	2.010	1.991	0.294	0.337	0.343	0.886	0.897
	3	7.058	5.847	5.358	2.552	2.038	1.981	0.358	0.306	0.331	0.919	0.934
	4	6.825	6.282	5.330	2.413	2.023	1.987	0.313	0.329	0.335	0.884	0.905
	5	6.343	6.663	5.377	2.582	1.986	2.018	0.309	0.324	0.320	0.858	0.929
18.23	1	7.522	6.531	5.575	2.697	2.123	2.074	0.321	0.315	0.332	0.893	0.904
	2	7.077	6.879	5.593	2.657	2.122	2.090	0.309	0.320	0.322	0.782	0.864
	3	6.556	7.314	5.573	2.889	2.081	2.115	0.300	0.322	0.313	0.829	0.940
	4	6.957	6.621	5.544	2.809	2.137	2.094	0.326	0.316	0.320	0.885	0.952
	5	6.745	7.436	5.539	2.765	2.083	2.120	0.279	0.336	0.325	0.829	0.909
22.44	1	8.501	7.025	5.936	3.174	2.275	2.209	0.350	0.296	0.318	0.874	0.911
	2	8.001	7.385	5.926	3.168	2.239	2.215	0.329	0.305	0.312	0.844	0.914
	3	7.155	8.234	5.940	3.018	2.204	2.308	0.285	0.314	0.307	0.813	0.902
	4	7.308	8.181	5.914	3.005	2.237	2.293	0.289	0.319	0.309	0.813	0.899
	5	7.286	7.361	5.883	3.328	2.258	2.249	0.341	0.302	0.297	0.849	0.981

tion in *XY*-plane and as explained for Case 1, the projected areas of fibres on *XZ* and *YZ* planes are approaching to be equal. Thus, contribution of fibre stiffness is almost equal in these planes, unlike in Case 1. However, for *YZ*-plane the projected area is almost same as in Case 1 for a given volume fraction. It is to be noted that the fibre itself is transversely isotropic in nature here. Due to this arrangement of fibres in RVEs and their transverse isotropic nature, the isotropy in *YZ* plane is affected. This can be seen through the decrement of parameter a_{YZ} in comparison to Case 1. This is reduced to a minimum of 83% for the studied volume fractions. On the contrary, this arrangement has led to an improvement in overall isotropic behaviour as can be seen through the values of parameter *a*. This value is above 91% for the volume fractions studied (See Table 11). Furthermore, as the volume fraction increases these properties also increase.

Table 11 represents the mean and standard deviation in effective property values of RVEs developed. The values of Young's moduli and shear moduli increase as the volume fraction increases. However, Poisson's ratios decrease slightly with the increase in volume fraction. In general, the standard deviation in the values of effective properties is less than 1 and increases as volume fraction is increased. The standard deviation values for Young's moduli in *X* and *Y* directions have comparatively larger scatter than remaining properties due to random orientation and distribution

Table 11
Average and standard deviation in effective properties of Case 2.

Property	V_f 15.43 (%)		V_f 19.63 (%)		V_f 22.44 (%)	
	Mean	SD	Mean	SD	Mean	SD
E_1 (GPa)	6.741	0.259	6.971	0.367	7.650	0.579
E_2 (GPa)	6.308	0.296	6.956	0.406	7.637	0.540
E_3 (GPa)	5.355	0.052	5.565	0.023	5.920	0.023
G_{12} (GPa)	2.540	0.164	2.764	0.092	3.139	0.133
G_{13} (GPa)	2.015	0.019	2.109	0.026	2.243	0.027
G_{23} (GPa)	1.996	0.015	2.099	0.019	2.255	0.045
v_{12}	0.326	0.029	0.307	0.019	0.319	0.030
v_{13}	0.321	0.014	0.322	0.008	0.307	0.009
v_{23}	0.329	0.011	0.322	0.007	0.309	0.008
a_{YZ}	0.884	0.022	0.844	0.045	0.838	0.026
a	0.923	0.022	0.914	0.034	0.921	0.034

of fibres in that direction (*XY*-plane). Further, as the volume fraction increases the scatter in the property values also increases. The variation in properties among different RVE models for a particular volume fraction is attributed to packing arrangement of fibres in RVEs. The very low value of standard deviation (less than 1%) among the property values indicates that the present approach is efficient in generating the RVEs such that predicted macroscopic behaviour is repetitive in nature for the given volume fraction for this case also.
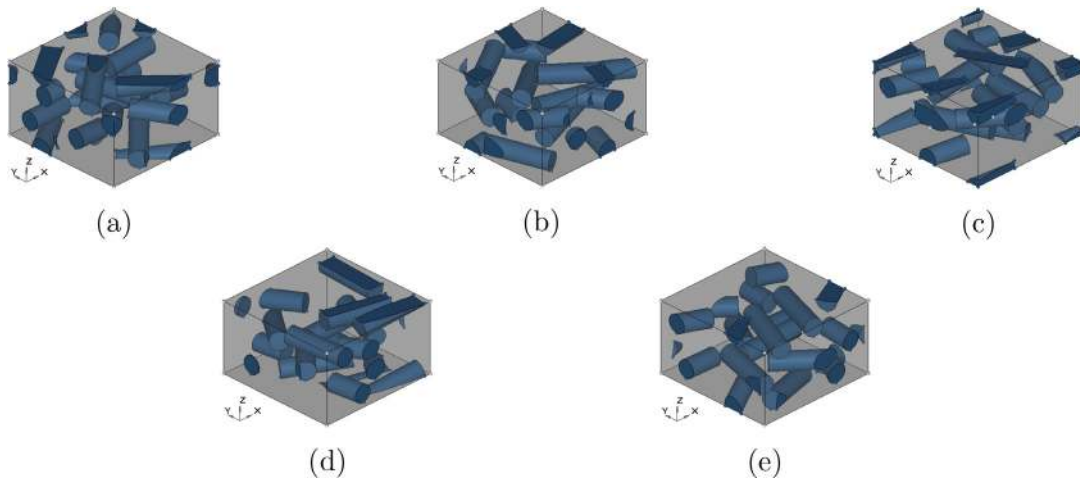
Fig. 18. RVEs for Case 3 with fibre volume fraction of 15.43%. (a) RVE 1, (b) RVE 2, (c) RVE 3, (d) RVE 4, (e) RVE 5.
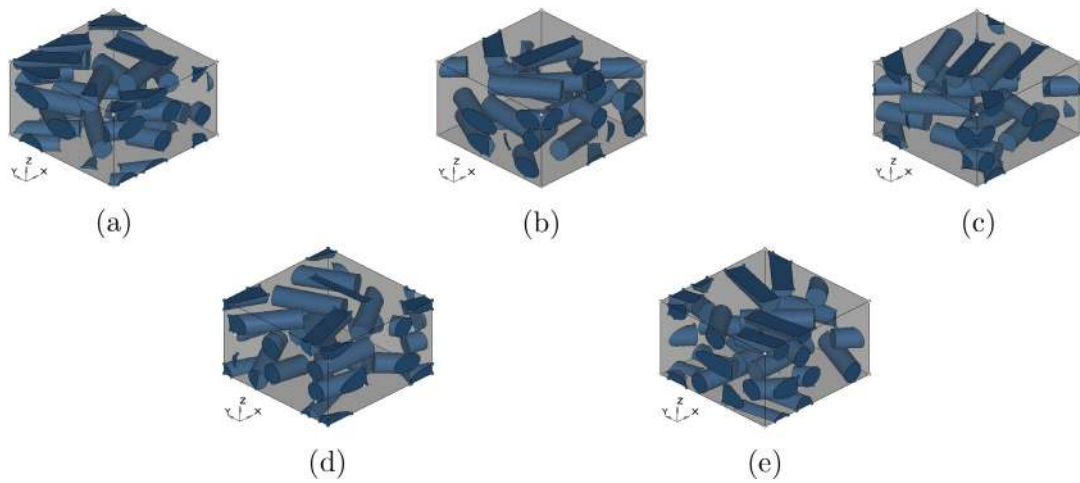

Fig. 19. RVEs for Case 3 and fibre volume fraction of 19.63%. (a) RVE 1, (b) RVE 2, (c) RVE 3, (d) RVE 4, (e) RVE 5.
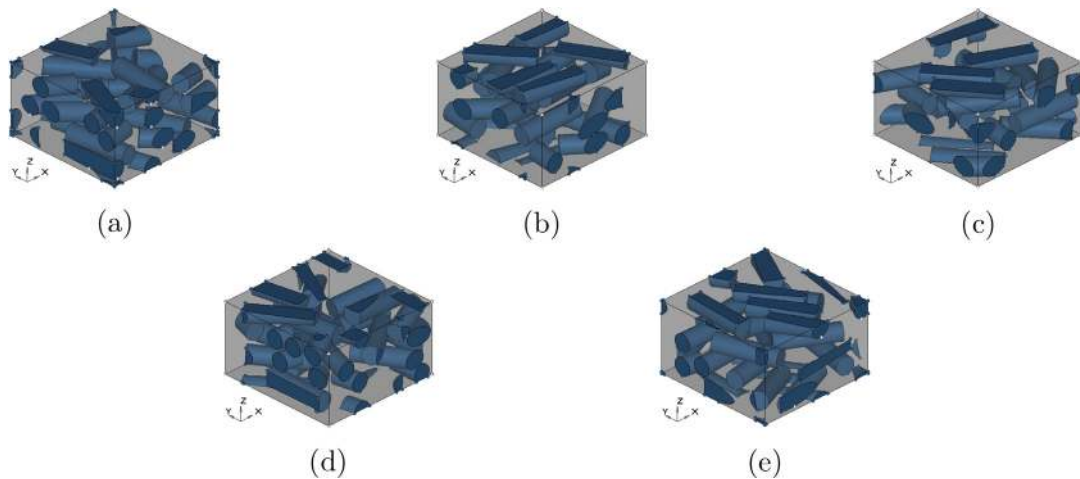

Fig. 20. RVEs for Case 3 with fibre volume fraction of 21.04%. (a) RVE 1, (b) RVE 2, (c) RVE 3, (d) RVE 4, (e) RVE 5.

3.3. Case 3: in-plane randomly oriented and out of plane partial randomly oriented fibres

In this section the RVEs generated with fibres randomly oriented in a plane and partially oriented in out of plane directions are analyzed for their effective properties. This case is a generaliza-tion of Case 2, indicating that RVE cannot have all the fibres ran-domly oriented in one plane only all the time and hence a small out of plane deviation is allowed. The procedure followed to gen-erate an RVE is same as in Case 2 and further allowing orientations of the fibres by $\pm 10°$ in *XZ*-plane. Here also the effect of volume fraction is studied by considering three different volume fractions.
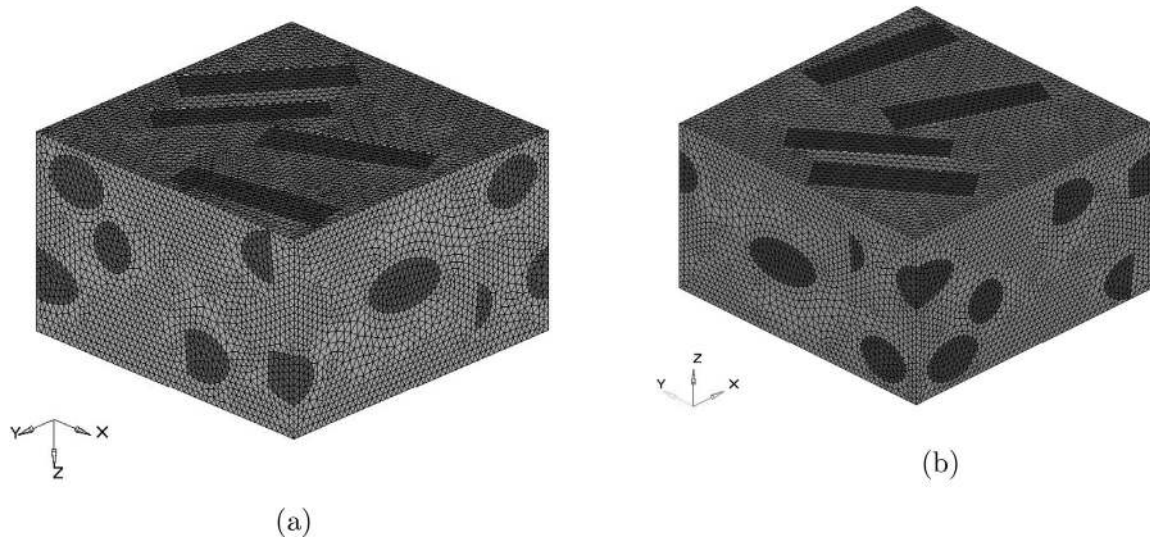
Fig. 21. A typical meshed RVE for Case 3. (a) Meshes on positive *x, y* and negative *z* faces, (b) meshes on negative *x, y* and positive *z* face.

Table 12
Properties of in-plane and partial out of plane orientation for short fibre composites: Case 3.

V_f (%)	Model	E_1 (GPa)	E_2 (GPa)	E_3 (GPa)	G_{12} (GPa)	G_{13} (GPa)	G_{23} (GPa)	ν_{12}	ν_{13}	ν_{23}	a_{YZ}	a
15.43	1	6.745	5.878	5.391	2.617	2.042	1.980	0.362	0.303	0.319	0.913	0.956
	2	6.824	6.037	5.335	2.542	2.020	1.986	0.333	0.318	0.332	0.914	0.934
	3	6.569	7.072	5.325	2.406	1.995	2.018	0.272	0.345	0.342	0.839	0.875
	4	6.365	6.946	5.377	2.363	1.995	2.025	0.287	0.338	0.323	0.839	0.884
	5	6.828	6.483	5.368	2.361	2.013	1.990	0.305	0.327	0.337	0.868	0.882
19.63	1	6.237	7.504	5.681	2.852	2.120	2.188	0.299	0.316	0.299	0.829	0.951
	2	6.873	7.430	5.675	2.812	2.149	2.163	0.296	0.324	0.314	0.835	0.918
	3	7.496	7.224	5.728	2.741	2.151	2.161	0.309	0.315	0.323	0.854	0.885
	4	7.812	6.392	5.646	2.805	2.214	2.109	0.343	0.310	0.327	0.913	0.924
	5	7.023	7.782	5.718	2.777	2.113	2.167	0.286	0.327	0.314	0.808	0.882
21.04	1	7.388	8.042	5.960	2.931	2.247	2.274	0.293	0.316	0.305	0.813	0.891
	2	8.834	7.328	5.856	2.833	2.299	2.240	0.287	0.330	0.342	0.884	0.851
	3	7.607	7.638	5.931	3.198	2.233	2.259	0.315	0.305	0.311	0.841	0.929
	4	7.053	8.721	5.940	2.866	2.224	2.296	0.259	0.329	0.307	0.778	0.866
	5	8.311	7.992	5.905	2.846	2.259	2.245	0.281	0.330	0.329	0.823	0.842

Table 13
Average and standard deviation in effective properties of Case 3.

Property	Vf 15.43 (%)		Vf 19.63 (%)		Vf 21.04 (%)	
	Mean	SD	Mean	SD	Mean	SD
E_1 (GPa)	6.666	0.198	7.088	0.606	7.839	0.722
E_2 (GPa)	6.483	0.531	7.267	0.528	7.944	0.521
E_3 (GPa)	5.359	0.028	5.690	0.033	5.918	0.040
G_{12} (GPa)	2.458	0.115	2.797	0.042	2.935	0.152
G_{13} (GPa)	2.013	0.020	2.149	0.040	2.252	0.029
G_{23} (GPa)	2.000	0.020	2.158	0.029	2.263	0.023
ν_{12}	0.312	0.036	0.307	0.022	0.287	0.020
ν_{13}	0.326	0.017	0.318	0.007	0.322	0.011
ν_{23}	0.331	0.010	0.315	0.011	0.319	0.016
a_{YZ}	0.875	0.037	0.847	0.039	0.827	0.038
a	0.906	0.036	0.912	0.028	0.875	0.035

The three volume fractions of 15.43%, 19.63% and 21.04% are studied for this case. For each volume fraction five different models of RVE have been generated. Fig. 18, Fig. 19 and Fig. 20 show the RVE models generated for 15.43%, 19.63% and 21.04% fibre volume fractions, respectively. Figure 21 shows an RVE meshed for finite element analysis.

The effective properties obtained for the RVE models have been reported in Table 12. Table 13 represents the mean and standard deviation in these effective properties. It is seen that effective properties from different RVEs for the respective volume fractions are close to each other. It can be observed that the Young's modulus in *z* direction, E_3 shows a slight increment in the values for respective volume fraction. This is due to partial orientation of fibres in that direction. This also affects the Young's moduli in *X* and *Y* directions and a small increment is also seen in these values in comparison to those reported for Case 2. Further, it is observed that the shear moduli G_{13} and G_{23} are again close to each other for respective RVEs of all volume fractions as in Case 2. However, the respective values are little lowered in comparison to those of Case 2. This is because of partial orientation of fibres in the *Z*-direction. The contribution coming from the fibre direction is now lesser. A similar behaviour is observed for G_{12} for the same reason.

From Table 13 it is seen that the effective properties of composite material developed increase as the volume fraction increases. This is due the fact that the contribution of the properties from fibre, particularly the ones in fibre direction increases as the fibre volume fraction increases. However, for the Poisson's ratios the values decrease as the fibre volume fraction increases. Again this is due to constraint imposed by fibre properties in fibre direction on the lateral expansion of the resulting composite.

Tables 12 and 13 give insight about the macroscopic behaviour of the resulting composites through the parameters a_{YZ} and a. The isotropy in *YZ*-plane, in general, is reduced in comparison to Case 2. Further, as the fibre volume fraction increases this value de-
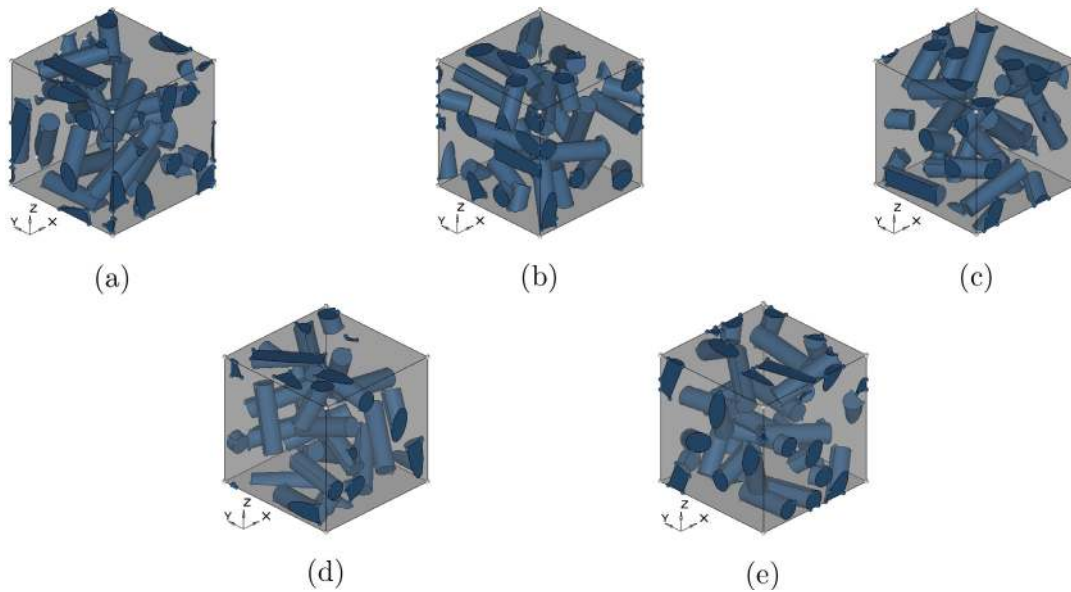
Fig. 22. RVEs for Case 4 with fibre volume fraction of 15.23%. (a) RVE 1, (b) RVE 2, (c) RVE 3, (d) RVE 4, (e) RVE 5.
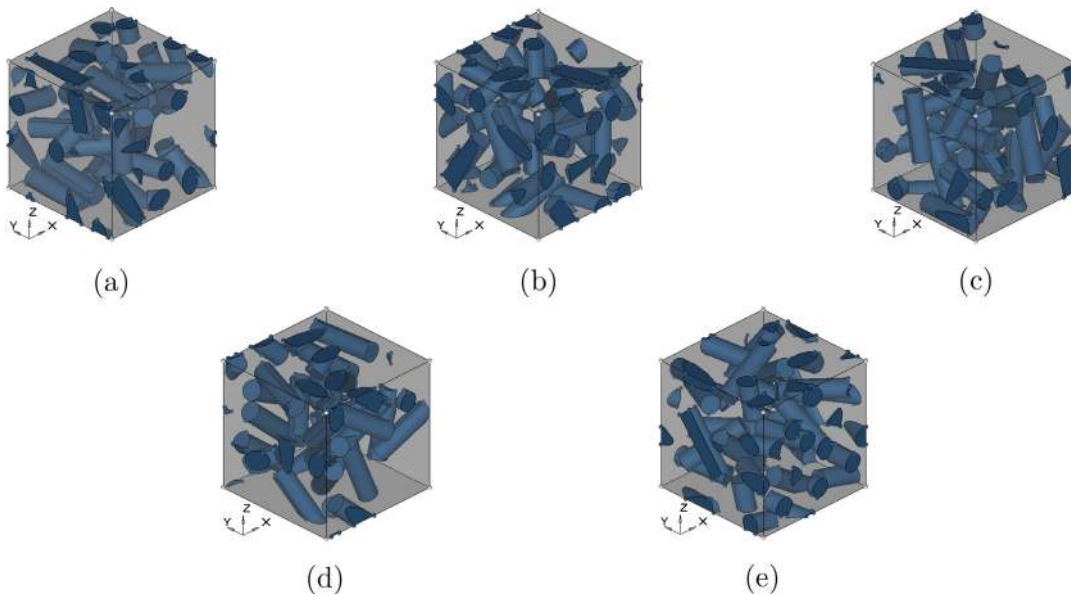

Fig. 23. RVEs for Case 4 with fibre volume fraction of 19.23%. (a) RVE 1, (b) RVE 2, (c) RVE 3, (d) RVE 4, (e) RVE 5.

creases. The parameter a_{YZ} is seen to have value above 0.82 for the volume fractions studied. Furthermore, the macroscopic isotropic behaviour represented by a is seen to reduce and also reduces with the increase in fibre volume fraction. Here, this parameter has a value above 0.87 for the volume fractions studied. The change in macroscopic behaviour in comparison to Case 2 is due to partial alignment of fibres in the Z-direction. Note that the volume fractions achieved in the RVEs of cases studied, that is Case 1, Case 2, etc. are very close but not the same.

3.4. Case 4: completely random oriented fibres

In this section, fibres are allowed to orient randomly in all planes inside an RVE. To generate the RVE, fibres are located one after the other at random locations and oriented randomly in-plane (*XY*-plane) and out of plane (*YZ*-plane). The geometric periodicity is maintained in RVEs and fibres are allowed neither to overlap nor to intersect each other. The fibre volume fractions con-

sidered for RVE generation with random oriented fibres are 15.23%, 19.23% and 21.64%. The RVEs generated are as shown in Figs. 22, 23, 24, respectively for these volume fractions. Five different models of RVE for each volume fraction considered have been created and their effective properties are obtained. A typical meshed RVE from this case has been shown in Fig. 25.

The effective stiffness tensors for the fibre volume fraction of 15.23%, as an example, are given in Table 14. The subscripts used with the stiffness tensor [*C*] denote the corresponding RVE of that volume fraction. From this table it is seen that the degree of anisotropy is not significant for this case also.

Table 15 presents the effective properties of individual RVE models considered for this case. It is observed from Table 15 that Young's moduli in all three directions of different RVEs for a particular volume fraction are almost equal. Furthermore, a similar observation can be made for shear moduli and Poisson's ratios. Mean and standard deviation in the values of the properties from these models have been calculated and reported in Table 16. It is inferred
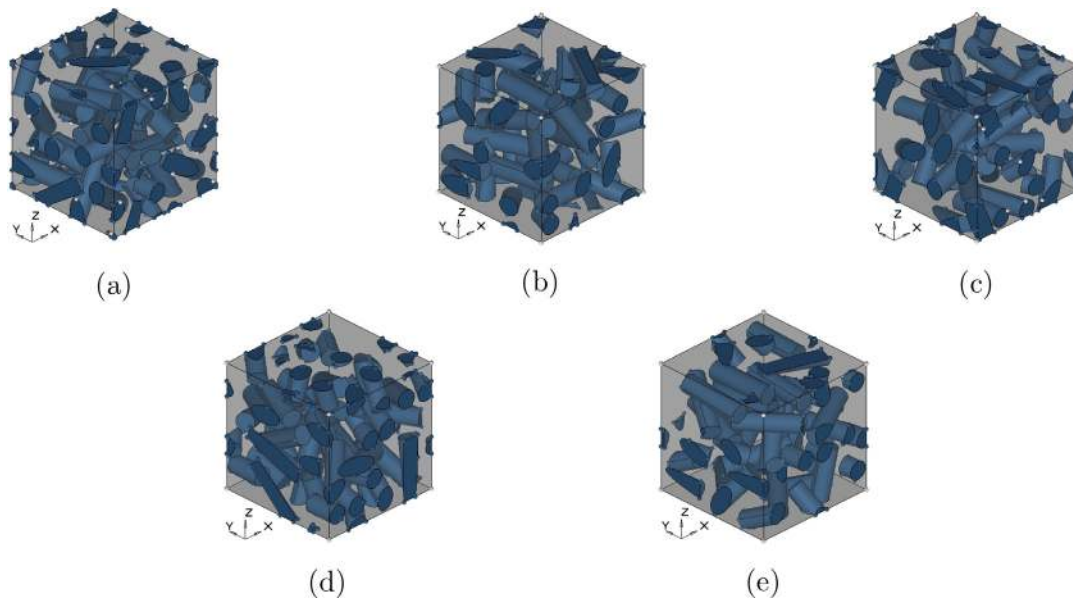
Fig. 24. RVEs for Case 4 with fibre volume fraction of 21.64%. (a) RVE 1, (b) RVE 2, (c) RVE 3, (d) RVE 4, (e) RVE 5.
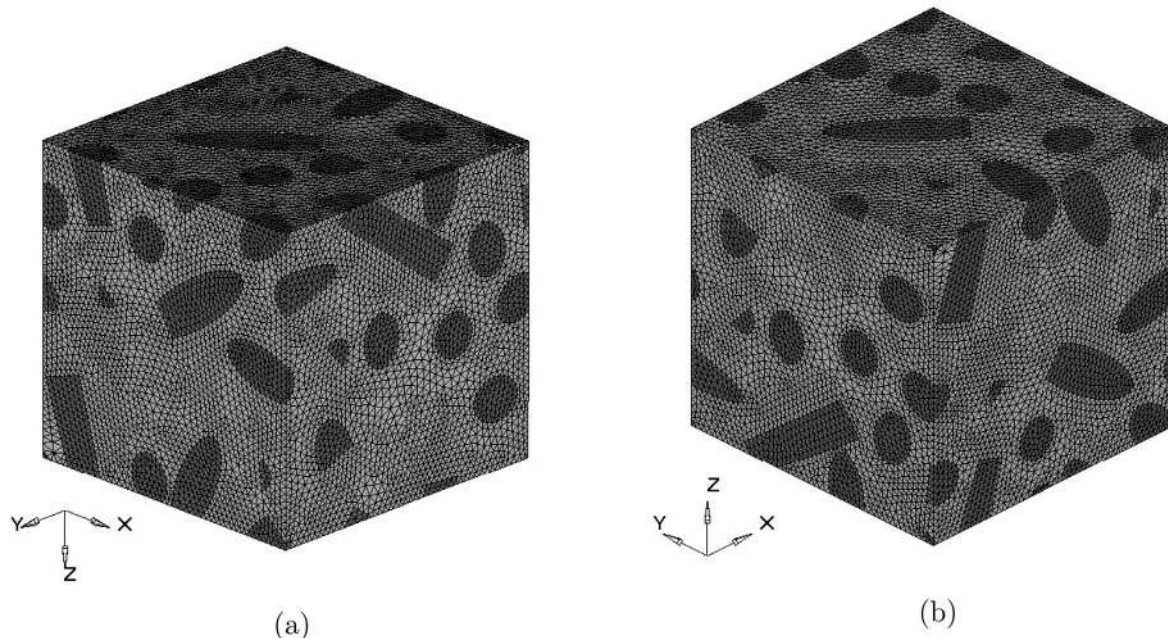

Fig. 25. A typical meshed RVE for Case 4. (a) Meshes on positive *x, y* and negative *z* faces, (b) meshes on negative *x, y* and positive *z* face.

from Table 16 that as the volume fraction increases the effective elastic moduli increase and Poisson's ratio decrease. The standard deviation for all properties is less than 1% for all volume fractions studied. This indicates that the deviation of effective properties of an individual model from the mean values is very less. This again indicates the efficacy of repetitiveness of the approach used to generate RVEs in predicting effective properties.

The parameters a_{YZ} and a reported in Table 15 and Table 16 show that their values are approaching to unity. Thus, it indicates that the overall macroscopic behaviour of the material is approaching to isotropic. This behaviour is as expected because the arrangement of fibres inside such a composite is completely random leading to equal distribution of their properties in all directions. However, it is seen that as the fibre volume fraction increases the values of these parameters decrease slightly.

It is seen that the parameter a_{YZ}, which is defined to denote the isotropy in *YZ* plane is approaching to unity for this case. It was seen earlier that for the Case 1 it also approached unity. Then for Case 2 and Case 3 it deviated from unity. It is to be noted that as the overall material behaviour is approaching to isotropic nature then in any plane it will behave isotropic in nature. Thus, this observation is consistent. One could have chosen any plane to check the isotropy in that plane. However, in the Case 1 the fibres were aligned normal to *YZ* plane, therefore, this plane was used to check the isotropy.

Remark 6. In general, it is seen that as the fibre volume fraction increases the SD in the effective property values increases. This is due to packing factor of fibre arrangement. In the present approach the fibres are added one after the other with the constraint that they do not touch other. This is implemented by controlling the

Table 14
Effective stiffness tensors for all fibres randomly arranged case with fibre volume fraction of 15.23% (Values in MPa).

$$[C]_1 = \begin{bmatrix} 7825 & 3452 & 3547 & 47 & 101 & 173 \\ & 7528 & 3457 & 0 & 35 & 78 \\ & & 7906 & 20 & 79 & 57 \\ & & & 2083 & 61 & 47 \\ & & & & 2130 & 24 \\ & & & & & 2090 \end{bmatrix}, \quad [C]_2 = \begin{bmatrix} 7605 & 3473 & 3455 & 1 & 44 & 83 \\ & 7761 & 3440 & 11 & 18 & 87 \\ & & 7992 & 48 & 64 & 15 \\ & & & 2075 & 10 & 8 \\ & & & & 2070 & 21 \\ & & & & & 2117 \end{bmatrix},$$

$$[C]_3 = \begin{bmatrix} 7748 & 3439 & 3562 & 0 & 0 & 129 \\ & 7592 & 3418 & 0 & 0 & 15 \\ & & 7880 & 0 & 0 & 7 \\ & & & 2044 & 0 & 3 \\ & & & & 2179 & 0 \\ & & & & & 2062 \end{bmatrix}, \quad [C]_4 = \begin{bmatrix} 7604 & 3411 & 3455 & 0 & 24 & 0 \\ & 7617 & 3481 & 0 & 36 & 0 \\ & & 8057 & 29 & 63 & 7 \\ & & & 2128 & 9 & 41 \\ & & & & 2060 & 0 \\ & & & & & 2060 \end{bmatrix},$$

$$[C]_5 = \begin{bmatrix} 7588 & 3386 & 3531 & 30 & 25 & 0 \\ & 7754 & 3423 & 60 & 0 & 0 \\ & & 7943 & 0 & 0 & 20 \\ & & & 2065 & 22 & 0 \\ & & & & 2114 & 13 \\ & & & & & 2046 \end{bmatrix}$$

Table 15
Properties of completely random orientated short fibre composites: Case 4.

V_f (%)	RVE No.	E_1 (GPa)	E_2 (GPa)	E_3 (GPa)	G_{12} (GPa)	G_{13} (GPa)	G_{23} (GPa)	ν_{12}	ν_{13}	ν_{23}	a_{YZ}	a
15.23	1	5.622	5.436	5.700	2.086	2.127	2.080	0.316	0.310	0.301	0.978	0.985
	2	5.483	5.633	5.858	2.115	2.070	2.075	0.316	0.296	0.290	0.936	0.964
	3	5.543	5.525	5.686	2.060	2.180	2.045	0.310	0.318	0.294	0.947	0.983
	4	5.520	5.512	5.873	2.060	2.060	2.128	0.314	0.293	0.298	0.977	0.967
	5	5.465	5.701	5.752	2.047	2.114	2.065	0.297	0.317	0.293	0.934	0.962
19.23	1	5.700	5.838	6.405	2.119	2.203	2.191	0.304	0.285	0.272	0.919	0.942
	2	5.884	5.921	6.121	2.151	2.237	2.264	0.294	0.297	0.299	0.981	0.966
	3	5.968	5.932	6.303	2.194	2.182	2.239	0.306	0.284	0.291	0.952	0.944
	4	5.858	5.886	6.070	2.133	2.395	2.193	0.294	0.317	0.289	0.948	0.984
	5	6.069	6.322	6.003	2.285	2.290	2.199	0.293	0.317	0.293	0.917	0.957
21.64	1	6.277	6.207	6.564	2.283	2.435	2.338	0.293	0.299	0.277	0.939	0.958
	2	6.093	6.631	6.245	2.396	2.353	2.359	0.280	0.309	0.289	0.938	0.971
	3	6.050	6.400	6.532	2.311	2.401	2.354	0.286	0.300	0.276	0.931	0.964
	4	5.848	6.407	6.785	2.338	2.288	2.433	0.293	0.275	0.272	0.946	0.959
	5	6.081	6.639	6.536	2.368	2.325	2.346	0.285	0.295	0.277	0.908	0.945

Table 16
Average and standard deviation in effective properties of Case 4.

Properties	V_f 15.23 (%)		V_f 19.23 (%)		V_f 21.64 (%)	
	Mean	SD	Mean	SD	Mean	SD
E_1 (GPa)	5.527	0.062	5.896	0.137	6.069	0.153
E_2 (GPa)	5.561	0.105	5.980	0.195	6.457	0.182
E_3 (GPa)	5.774	0.087	6.180	0.168	6.532	0.192
G_{12} (GPa)	2.074	0.027	2.176	0.067	2.339	0.044
G_{13} (GPa)	2.110	0.048	2.261	0.085	2.361	0.058
G_{23} (GPa)	2.078	0.031	2.217	0.033	2.366	0.038
ν_{12}	0.311	0.008	0.298	0.006	0.288	0.006
ν_{13}	0.307	0.011	0.300	0.016	0.296	0.013
ν_{23}	0.295	0.004	0.289	0.010	0.278	0.006
a_{YZ}	0.954	0.022	0.944	0.026	0.933	0.015
a	0.972	0.011	0.958	0.017	0.959	0.009

distance between the closest points on the adjacent fibres. Further, the dimensions of the RVE chosen are fixed for all fibre volume fractions. Thus, these constraints restrict the arrangement of fibres that are added at later stages. In turn, it causes the deviation in the effective properties. However, this deviation for all the cases studied here is less than 1% indicating the efficacy of the approach developed for the RVE generation.

4. Conclusions

In the present study a statistical representation of the short fibre composite material at microscale through a representative volume element has been developed using random sequential adsorption technique. A numerical tool developed using MATLAB generates the RVE for a maximum volume fraction of 22.44% by maintaining the distance between adjacent two fibres as 0.001 times the side length of the RVE. Geometric periodicity is implemented while developing the RVE to ensure the continuity of the fibres across the neighbouring RVEs. Mathematical theory of homogenization has been implemented for the prediction of effective stiffness. Here, four different cases of fibre arrangements in RVE had been modeled and analyzed for their effective properties. For each case of fibre arrangement, RVEs with three/four different fibre volume fractions are evaluated for effective stiffness. To study the effectiveness of RVE generation algorithm in terms of repetitiveness of predicted stiffness, five RVEs are studied for each fibre volume fraction. The results of the case where all fibres are aligned in one direction are compared with those of Mori–Tanaka and Halpin–Tsai methods. A brief convergence study with respect to number of elements in finite element discretization is also carried out.

The key conclusions that can be made from this study are listed as:

1. The results obtained from the methods developed using RVE are compared with analytical or non-RVE methods like Halpin–Tsai and Mori–Tanaka method for Case 1 with in-plane aligned fibres. The effective properties obtained from RVE method have good correlation with Halpin–Tsai and Mori–Tanaka method. The effective property values from Halpin–Tsai method for a particular volume fraction are close to that of mathematical homogenization method for almost all engineering constants, except out of plane Poisson's ratio ν_{23}.

2. When the volume fraction increases, the effective properties increases in both RVE and non-RVE methods, also the percentage difference with two non RVE methods also increases. Longitudinal Young's modulus from present study has 6.5% to 11% and 6.5% to 12% difference with respect to Mori–Tanaka and Halpin–Tsai methods, respectively. The transverse Young's modulus has approximately 7.5% to 12% and 2% to 4.5% difference with Mori–Tanaka and Halpin–Tsai methods, respectively. For transverse shear modulus, the percentage difference is 3% to 10.5% and 3% to 8% with respect to Mori–Tanaka and Halpin–Tsai methods, respectively.

3. Poisson's ratio has 0.15% to 4% and 4% to 9% deviation, except for ν_{23} which has 2% to 7% and 22% to 25.8% deviation with respect to Mori–Tanaka and Halpin–Tsai methods, respectively. This large deviation is due to location and orientation of fibres in RVE, volume fraction and aspect ratio of fibres.

4. The effective properties obtained from mathematical theory of homogenization for different RVEs for a particular case ensures the reliability of RSA algorithm developed and consistently predicts the effective material properties. Standard deviation values on effective properties of RVEs developed is either close to zero or less than 1%, which also indicates the efficacy of the algorithm developed for RVE generation in fulfilling the requirement of repetitiveness of the resulting effective material.

5. RVEs with in-plane aligned fibres behave like a transversely isotropic material at macrolevel in a plane perpendicular to the direction of fibre alignment due to fibre packing arrangement in RVE, whereas RVEs with random in-plane orientation at microscale behave like a transversely isotropic material at macroscale in another particular plane. Further, RVEs with random in-plane orientation and partial out of plane orientation of fibres also behave closely to transversely isotropic nature. Finally, RVEs with completely random orientation of all fibres at microscale, behaves like an isotropic material at macrolevel.

As the restriction of random distribution of fibres in an RVE is relaxed more and more the macroscopic behaviour changes from transverse isotropy, with respect to a particular plane, to fully isotropic. For in-plane aligned fibres in RVE, the material developed is almost 98-99% close to transverse isotropy and 73-78% overall isotropy in nature. The materials with in-plane randomly oriented fibres, the material is more than 83% close to transversely isotropic behaviour and about 91% overall isotropic behaviour. The RVEs with randomly in-plane fibre orientation and partial out of plane fibre orientation exhibited more than 82% closeness to transversely isotropic behaviour and over 87% overall isotropic behaviour. Finally, the RVEs with completely random oriented fibres exhibited more than 90% closeness to transversely isotropic behaviour and more than 95% overall isotropic behaviour of the material.

6. As fibre volume fraction increases the parameters defined to represent degree of transverse isotropy, a_{YZ}, and degree of overall isotropy, a, decrease, in general, for all four cases studied. The maximum change of 14.87% and 11.90%, respectively was seen for Case 3 with fibres arranged randomly in in-plane and partial out of plane random arrangement. This is due to packing geometry factor.

7. Stiffness tensors showed negligible anisotropy and were symmetric for each of the RVE studied for all the cases.

Appendix A. Methods for predicting effective stiffness

In this section three different methods are explained which are used to estimate the effective stiffness tensor. These methods are: Mathematical theory of homogenization (Hollister and Kikuchi, 1992), Halpin–Tsai technique (Halpin and Kardos, 1976; Tucker and Liang, 1999) and Mori–Tanaka (Mori and Tanaka, 1973;

Mura, 1987) method. The former one is an RVE based method and the later two are non RVE methods.

A1. Mathematical theory of homogenization

Homogenization theory is developed from studies of partial differential equations with rapidly varying coefficients. To represent a complex rapidly varying medium with slowly varying medium, in which fine scale structure is averaged in an approximate way, the following two explicit assumptions are made in homogenization theory.

1. Fields vary on multiple scales due to existence of microstructure.
2. Microstructure is spatially periodic.

The relevant field variables are approximated by an asymptotic expansion as

$$u_i^\eta(x_i, y_i) = u_{0i}(x_i, y_i) + \eta u_{1i}(x_i, y_i) + \eta^2 u_{2i}(x_i, y_i) + \dots \quad (A.1)$$

where u_i^η is the exact value of field variable, u_{0i} is the macroscopic value of field variable, u_{1i}; u_{2i}, etc. are perturbations in field variables due to microstructure, x_i and y_i are the global level and micro level coordinates, respectively and η is the ratio of microstructure size to the total size of analysis region $\left(\eta = \frac{x_i}{y_i}\right)$.

Classical arguments of oscillating functions result that the macroscopic stress and strain tensor must be the average of microscopic stress and strain quantities. Thus,

$$\overline{\sigma}_{ij} = \frac{1}{|V_{RVE}|} \int_{V_{RVE}} \sigma_{ij}(\mathbf{x})\, dV \quad \text{and} \quad \overline{\epsilon}_{ij} = \frac{1}{|V_{RVE}|} \int_{V_{RVE}} \epsilon_{ij}(\mathbf{x})\, dV$$
(A.2)

where, $\overline{\sigma}_{ij}$, $\overline{\epsilon}_{ij}$ are the average stresses and average strains and σ_{ij} and ϵ_{ij} are the local stresses and local strains in RVE and V_{RVE} is the volume of RVE.

Substituting the asymptotic expansion of Eq. (A.1) in terms of strains and neglecting the higher order terms of the standard weak form of equilibrium equations governing the mechanical behaviour of the composite material at different levels of structure, we get strains as

$$\epsilon_{ij}(\mathbf{u}) = \frac{1}{2}\left[\left(\frac{\partial u_{0i}}{\partial x_j} + \frac{\partial u_{0j}}{\partial x_i}\right) + \left(\frac{\partial u_{1i}}{\partial y_j} + \frac{\partial u_{1j}}{\partial y_i}\right)\right] \quad (A.3)$$

The components of strain tensor can be written as

$$\epsilon_{ij}(\mathbf{u}) = \overline{\epsilon}_{ij} + \epsilon_{ij}^* \quad (A.4)$$

where,

$$\overline{\epsilon}_{ij}(\mathbf{u}) = \frac{1}{2}\left[\frac{\partial u_{0i}}{\partial x_j} + \frac{\partial u_{0j}}{\partial x_i}\right] \quad \text{and} \quad \epsilon_{ij}^*(\mathbf{u}) = \frac{1}{2}\left[\frac{\partial u_{1i}}{\partial y_j} + \frac{\partial u_{1j}}{\partial y_i}\right]$$
(A.5)

wherein, ϵ_{ij} is the local or microstructural strain tensor, $\overline{\epsilon}_{ij}$ is the average or macroscopic strain tensor and ϵ_{ij}^* is the fluctuating microstructural strain tensor which is assumed to vary periodically. Similarly, the virtual displacement $\mathbf{v}$ and hence the virtual strain $\epsilon_{ij}(\mathbf{v})$ is also expanded asymptotically as a function of x and y, neglecting the higher order terms. The resulting components of strain tensor can be written as

$$\epsilon_{ij}(\mathbf{v}) = \epsilon_{ij}^0 + \epsilon_{ij}^1 \quad (A.6)$$

where,

$$\epsilon_{ij}^0(\mathbf{v}) = \frac{1}{2}\left[\frac{\partial v_{0i}}{\partial x_j} + \frac{\partial v_{0j}}{\partial x_i}\right] \quad \text{and} \quad \epsilon_{ij}^1(\mathbf{v}) = \frac{1}{2}\left[\frac{\partial v_{1i}}{\partial y_j} + \frac{\partial v_{1j}}{\partial y_i}\right] \quad (A.7)$$

The expanded forms of strain tensors are substituted in standard weak form of equilibrium equations given by

$$\int_{\Omega^\eta} C_{ijkl}\, \epsilon_{ij}(\mathbf{v})\, \epsilon_{kl}(\mathbf{u})\, d\Omega^\eta = \int_\Gamma t_i\, v_i\, d\Gamma \tag{A.8}$$

where, Ω^η represents the total of macroscopic and microscopic domain of the composite materials, Γ is the macroscopic domain boundary and traction t_i is applied only to boundary of composite material. Substituting the expanded strain tensors in Eq. (A.8) yields

$$\int_{\Omega^\eta} C_{ijkl} \left(\epsilon_{ij}^0(\mathbf{v}) + \epsilon_{ij}^1(\mathbf{v}) \right) \left(\overline{\epsilon}_{kl}(\mathbf{u}) + \epsilon_{kl}^*(\mathbf{u}) \right) d\Omega^\eta = \int_\Gamma t_i\, v_i\, d\Gamma \tag{A.9}$$

Since $\mathbf{v}$ is an arbitrary function, it varies either on microscopic level or macroscopic level. If $\mathbf{v}$ varies on microscopic level, keeping constant in macroscopic level (yielding $\epsilon_{ij}^0(\mathbf{v}) = 0$), along with periodically varying of $\epsilon_{kl}^*(\mathbf{u})$ leads the microscopic equilibrium. The Eq. (A.9) is rewritten assuming η goes to zero in the limit, as

$$\int_\Omega \frac{1}{V_{RVE}} \int_{V_{RVE}} C_{ijkl} \left(\epsilon_{ij}^1(\mathbf{v}) \right) \left(\overline{\epsilon}_{kl}(\mathbf{u}) + \epsilon_{kl}^*(\mathbf{u}) \right) dV_{RVE}\, d\Omega = 0 \tag{A.10}$$

If $\mathbf{v}$ varies only on macroscopic level, keeping constant in microscopic level (giving $\epsilon_{ij}^1(\mathbf{v}) = 0$), along with periodically varying of $\epsilon_{kl}^*(\mathbf{u})$ leads the macroscopic equilibrium. Then Eq. (A.9) is rewritten, assuming η goes to zero in the limit, as

$$\int_\Omega \frac{1}{V_{RVE}} \int_{V_{RVE}} C_{ijkl} \left(\epsilon_{ij}^0(\mathbf{v}) \right) \left(\overline{\epsilon}_{kl}(\mathbf{u}) + \epsilon_{kl}^*(\mathbf{u}) \right) dV_{RVE}\, d\Omega = \int_\Gamma t_i\, v_i\, d\Gamma \tag{A.11}$$

Eq. (A.10) will be satisfied, if the integral over RVE is zero. This means Eq. (A.10) may be written as

$$\int_{V_{RVE}} C_{ijkl}\, \epsilon_{ij}^1(\mathbf{v})\, \epsilon_{kl}^*(\mathbf{u})\, dV_{RVE} = - \int_{V_{RVE}} C_{ijkl}\, \epsilon_{ij}^1(\mathbf{v})\, \overline{\epsilon}_{kl}(\mathbf{u})\, dV_{RVE} \tag{A.12}$$

In general, $\overline{\epsilon}_{kl}(\mathbf{u})$ is not known apriori. For linear problem in 3D, $\overline{\epsilon}_{kl}(\mathbf{u})$ can be written as a linear combination of unit strains as given below.

$$\overline{\epsilon}_{pm}^{11} = -\begin{bmatrix} 1 & 0 & 0 \\ 0 & 0 & 0 \\ 0 & 0 & 0 \end{bmatrix}, \quad \overline{\epsilon}_{pm}^{12} = -\begin{bmatrix} 0 & 1 & 0 \\ 0 & 0 & 0 \\ 0 & 0 & 0 \end{bmatrix},$$

$$\overline{\epsilon}_{pm}^{13} = -\begin{bmatrix} 0 & 0 & 1 \\ 0 & 0 & 0 \\ 0 & 0 & 0 \end{bmatrix},$$

$$\overline{\epsilon}_{pm}^{21} = -\begin{bmatrix} 0 & 0 & 0 \\ 1 & 0 & 0 \\ 0 & 0 & 0 \end{bmatrix}, \quad \overline{\epsilon}_{pm}^{22} = -\begin{bmatrix} 0 & 0 & 0 \\ 0 & 1 & 0 \\ 0 & 0 & 0 \end{bmatrix},$$

$$\overline{\epsilon}_{pm}^{23} = -\begin{bmatrix} 0 & 0 & 0 \\ 0 & 0 & 1 \\ 0 & 0 & 0 \end{bmatrix},$$

$$\overline{\epsilon}_{pm}^{31} = -\begin{bmatrix} 0 & 0 & 0 \\ 0 & 0 & 0 \\ 1 & 0 & 0 \end{bmatrix}, \quad \overline{\epsilon}_{pm}^{32} = -\begin{bmatrix} 0 & 0 & 0 \\ 0 & 0 & 0 \\ 0 & 1 & 0 \end{bmatrix},$$

$$\overline{\epsilon}_{pm}^{33} = -\begin{bmatrix} 0 & 0 & 0 \\ 0 & 0 & 0 \\ 0 & 0 & 1 \end{bmatrix}$$

By applying the symmetry of strain states and substituting the unit strains on the right hand side of Eq. (A.12), it gives a stress tensor as

$$\sigma_{ij}^{*kl} = C_{ijpm}\, \overline{\epsilon}_{pm}^{kl} \tag{A.13}$$

A set of six auxiliary problems have to be solved to obtain all the components for $\epsilon_{pm}^{*kl}(\mathbf{u})$ in Eq. (A.12). These are

$$\int_{V_{RVE}} C_{ijkl}\, \epsilon_{ij}^1(\mathbf{v})\, \epsilon_{pm}^{*kl}(\mathbf{u})\, dV_{RVE} = \int_{V_{RVE}} \epsilon_{ij}^1(\mathbf{v})\, \sigma_{ij}^{*kl}\, dV_{RVE} \tag{A.14}$$

To ensure periodicity of strain field ϵ_{pm}^{*kl} in Eq. (A.12) the value of ϵ_{ij}^* for any arbitrary $\overline{\epsilon}_{kl}$ can be written as

$$\epsilon_{ij}^* = -\epsilon_{ij}^{*kl}\, \overline{\epsilon}_{kl} \tag{A.15}$$

From classical arguments, the relationship between local RVE strain and the average strain can be written as

$$\epsilon_{ij} = M_{ijkl}\, \overline{\epsilon}_{kl} \tag{A.16}$$

where, M_{ijkl} is local structural tensor which can be obtained by using Eq. (A.15) and solving for M_{ijkl} leads to

$$M_{ijkl} = \frac{1}{2} \left(\delta_{ik}\delta_{jl} + \delta_{il}\delta_{jk} \right) - \epsilon_{ij}^{*kl} \tag{A.17}$$

where, δ_{ij} is the Kronecker delta.

The effective stiffness tensor which relates average stress and average strain can be calculated from M_{ijkl} by applying Hooke's law at microscopic level and integrating it over the volume of RVE and then divide by the volume of RVE. Thus,

$$\overline{\sigma}_{ij} = \frac{1}{|V_{RVE}|} \int_{V_{RVE}} C_{ijpm}\, M_{pmkl}\, dV_{RVE}\, \overline{\epsilon}_{kl} \tag{A.18}$$

from which the effective stiffness tensor can be written as

$$\overline{C}_{ijkl} = \frac{1}{|V_{RVE}|} \int_{V_{RVE}} C_{ijpm}\, M_{pmkl}\, dV_{RVE} \tag{A.19}$$

A2. Halpin–Tsai method

The key point of this section is to give a brief description about the formulation of Halpin–Tsai technique used to estimate the properties of aligned short fibre composites.

The works of Hill (1964) and Hermans (1967) were employed to derive Halpin–Tsai (Ashton et al., 1969) equations for continuous fibre composites. However, (Kerner, 1956) suggested that Halpin–Tsai form of equations can also be used for particulate composite. A detailed derivation of Halpin–Tsai formulation is explained by Halpin and Kardos (1976). A short description of formulation has been explained in this section.

A2.1. Young's modulus along fibre direction

Halpin–Tsai expressed longitudinal Young's modulus for aligned short fibre composite as follows

$$\frac{E_{11}}{E_m} = \frac{\left(1 + \zeta\, \eta V_f \right)}{\left(1 - \eta V_f \right)} \tag{A.20}$$

where,

$$\eta = \frac{\left(\frac{E_{1f}}{E_m} - 1 \right)}{\left(\frac{E_{1f}}{E_m} + 1 \right)} \quad \text{and} \quad \zeta = 2 * AR \tag{A.21}$$

where, E_{11} is longitudinal Young's modulus of composite along fibre direction, E_{1f} is Young's modulus of fibre in longitudinal direction, E_m is Young's modulus of matrix material, η is a parameter that depends on the matrix Poisson's ratio and on the particular elastic property being considered, V_f is the fibre volume fraction

of composite material and AR is the aspect ratio of fibre. The parameter ζ is a measure of reinforcement geometry and depends on loading condition. In general, for short fibre composites, the value of ζ lies between 0 and ∞. The aspect ratio, AR is defined as $AR = \frac{l_f}{d_f}$, where l_f is the length of the RVE and d_f is the diameter of the fibre.

A2.2. Young's modulus transverse to fibre direction

Halpin–Tsai method suggests that Young's modulus in transverse direction weakly depends on fibre aspect ratio and hence, the above equations can be used to obtain the transverse properties by letting $AR = 1$.

A2.3. Shear modulus estimation

Similar to transverse Young's modulus, aspect ratio does not affect the shear modulus. The shear modulus G_{12} is given by the relation

$$\frac{G_{12}}{G_m} = \frac{\left(1 + \zeta \, \eta \, V_f\right)}{\left(1 - \eta \, V_f\right)} \tag{A.22}$$

where, G_{12} is shear modulus of composite in 1-2 plane, G_m is shear modulus of matrix material. The parameter η is given as

$$\eta = \frac{\left(\frac{G_f}{G_m} - 1\right)}{\left(\frac{G_f}{G_m} + \zeta\right)} \tag{A.23}$$

Here, G_f is the corresponding fibre shear modulus. Further, $\zeta = 1$ is used. Similar relations can be used to determine G_{13} and G_{23}.

A2.4. Poisson's ratio estimation

Poisson's ratio of short fibre composite is bounded between a particulate composite and continuous fibre composite, which is independent of aspect ratio of fibre. Hence, rule of mixture can be applied to determine the properties. The major Poisson's ratio is given as

$$\nu_{12} = V_f \, \nu_f + V_m \, \nu_m \tag{A.24}$$

Here, ν_f and ν_m are the corresponding Poisson's ratios of fibre and matrix materials, respectively. Similar relations can be used to determine ν_{13} and ν_{23}.

A3. Mori–Tanaka method

In this section, the formulation of Mori–Tanaka technique (Mori and Tanaka, 1973; Mura, 1987) used to estimate the properties of oriented cylindrical short fibre composites is reviewed briefly.

Mori–Tanaka technique is one of the approximation method used to estimate the effective properties based on Eshelby's elasticity solution (Eshelby, 1957) for inhomogeneous inclusion in an infinite medium. The key assumption in this model is that the average strain in fibre is related to average strain in matrix by using a fourth order strain concentration tensor. Initially, Eshelby solved for a homogeneous inclusion of a prolate ellipsoid of revolution with semi-major axis a_1 and semi-minor axes a_2 and a_3 in an infinite matrix. It was concluded that within an inclusion the total strain $\boldsymbol{\epsilon}$ is uniform and related to transformation strain $\boldsymbol{\epsilon}^T$ by

$$\boldsymbol{\epsilon} = \boldsymbol{E}\boldsymbol{\epsilon}^T \tag{A.25}$$

where, $\boldsymbol{E}$ is known as Eshelby tensor. The individual components of Eshelby tensor are given in the following.

$$S_{iiii} = \frac{3}{8\pi\left(1 - \nu\right)} a_i^2 I_{ii} + \frac{\left(1 - 2\nu\right)}{8\pi\left(1 - \nu\right)} I_i$$

$$S_{iijj} = \frac{1}{8\pi\left(1 - \nu\right)} a_j^2 I_{ij} - \frac{\left(1 - 2\nu\right)}{8\pi\left(1 - \nu\right)} I_i$$

$$S_{iikk} = \frac{1}{8\pi\left(1 - \nu\right)} a_3^2 I_{ik} - \frac{\left(1 - 2\nu\right)}{8\pi\left(1 - \nu\right)} I_i$$

$$S_{ijij} = \frac{\left(a_i^2 + a_j^2\right)}{16\pi\left(1 - \nu\right)} I_{ij} + \frac{\left(1 - 2\nu\right)}{16\pi\left(1 - \nu\right)}\left(I_i + I_j\right)$$

$$S_{iiij} = S_{ijjk} = S_{ijkj} = 0 \tag{A.26}$$

where i, j, k varies from 1, 2, 3 in cyclic permutation. I_i and I_{ij} are the special elementary functions for inclusion of prolate spheroid in shape with $a_1 > a_2 = a_3$ which can be approximated for short cylindrical fibre considered in this study. The detailed derivation can be seen in Mura (1987). The terms used in above equation are given as

$$I_2 = I_3 = \frac{2\pi a_1 a_3^2}{\left(a_1^2 - a_3^2\right)^{3/2}}\left\{\frac{a_1}{a_3}\left(\frac{a_1^2}{a_3^2} - 1\right)^{1/2} - \cosh^{-1}\left(\frac{a_1}{a_3}\right)\right\}$$

$$I_1 = 4\pi - 2 \times I_2$$

$$I_{12} = I_{13} = \frac{\left(I_2 - I_1\right)}{\left(a_1^2 - a_2^2\right)}$$

$$I_{11} = \frac{4 \times \pi}{3 \times a_1^2} - \frac{2}{3} I_{12}$$

$$I_{22} = I_{33} = I_{23} = \frac{\pi}{a_2^2} - \frac{\left(I_2 - I_1\right)}{4\left(a_1^2 - a_2^2\right)} \tag{A.27}$$

Substituting Eq. (A.27) in Eq. (A.26), Eshelby tensor for homogeneous inclusion is obtained.

For an inhomogeneous inclusion in an infinite matrix, strain concentration tensor for Eshelby's equivalent inclusion can be obtained by using dilute Eshelby model as

$$\boldsymbol{A}^{Eshelby} = \left[\boldsymbol{I} + \boldsymbol{E}\boldsymbol{S}^m\left(\boldsymbol{C}^f - \boldsymbol{C}^m\right)\right]^{-1} \tag{A.28}$$

where, $\boldsymbol{C}^f$ and $\boldsymbol{C}^m$ are the stiffness tensors for fibre and matrix materials, respectively and $\boldsymbol{S}^m$ is the compliance tensor for matrix material. This formulation was used in Hill's approach by Russel (1973) to estimate the properties of aligned fibre composites. When many inclusions are immersed in matrix, strain concentration tensor, reformulated by Mori–Tanaka, is given as

$$\boldsymbol{A}^{MT} = \boldsymbol{A}^{Eshelby}\left[\left(1 - \nu_f\right)\boldsymbol{I} + \nu_f\boldsymbol{A}^{Eshelby}\right]^{-1} \tag{A.29}$$

By using Eq. (A.29) and fibre and matrix properties, effective stiffness tensor can be expressed as

$$\boldsymbol{C} = \boldsymbol{C}^m + \nu_f\left(\boldsymbol{C}^f - \boldsymbol{C}^m\right)\boldsymbol{A}^{MT} \tag{A.30}$$

By inverting effective stiffness tensor, effective compliance tensor is obtained, which gives the relations for effective engineering constants.

Appendix B. Finite element implementation of mathematical homogenization theory

In the present study, an in-house finite element code is developed to determine the homogenized properties of composite materials using mathematical theory of homogenization. The RVEs are discretized with linear tetrahedron elements. The commercial meshing software HYPERMESH® is used to discretize the RVEs. A displacement based finite element formulation with three displacement variables at each node has been implemented (see Cook et al., 2002 for more details).

In the following, the implementation of periodic boundary condition and post-processing of the results (displacement vector) to get the effective stiffness tensor is presented in brief.
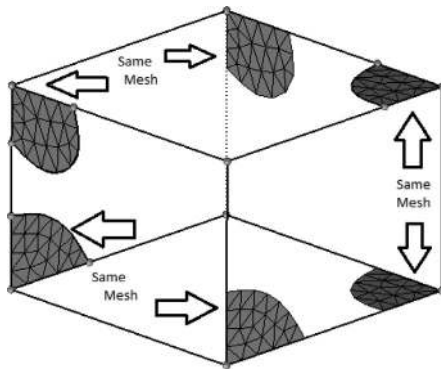
Fig. 26. An RVE with periodic mesh.

B1. Implementation of periodic boundary condition

Effective material properties of an RVE can be computed by ensuring the repeatability of boundary conditions to make ϵ_{ij}^{*kl} periodic in Eq. (A.14). The periodic boundary condition is implemented as follows.

1. Creating identical mesh on opposite faces of RVE, leading the nodes on opposite faces to have same coordinates tangential to face as shown in Fig. 26. Furthermore, these nodes are given same global numbers.
2. Element stiffness matrix and load vector assembling has been done as per the above criteria indicating identical displacements on opposite faces of an RVE.
3. Finally, to constrain the rigid body motion, the displacement at one of the node has to be fixed.

B2. Post processing

Once the weak form of equilibrium equation has been solved for six different loading cases individually, the fluctuating strain tensor ϵ_{ij}^{*kl} are evaluated at each integration point. These are used to construct the microstructural strain tensor M_{ijkl}. Then the effective stiffness tensor $\overline{C}_{ijkl}$ can be found by integrating over the discretized RVE and then divided by total volume of RVE as

$$\overline{\mathbf{C}} = \frac{1}{V_{RVE}} \sum_{i=1}^{NELEM} \sum_{j=1}^{NINT} [C] [M] |\mathbf{J}| \, w_j \tag{B.1}$$

where $\mathbf{C}$ is the constituent stiffness tensor, $\mathbf{M}$ is microstructural strain tensor, $|\mathbf{J}|$ is the determinant of the Jacobian, *NELEM* is number of elements in RVE, w_j are the weights and *NINT* is the number of integration points used in numerical integration.

References

Advani, S.G., Tucker III, C.L., 1987. The use of tensors to describe and predict fiber orientation in short fiber composites. J. Rheol. 31, 751–784.

Ashton, J.E., Halpin, J.C., Petit, P.H., 1969. Primer on Composite Materials: Analysis. Technomic Publishing Co, Stanford, Conn., USA.

Benveniste, Y., 1987. A new approach to the application of Mori–Tanaka's theory in composite materials. Mech. Mater. 6, 147–157.

Berger, H., Kari, S., Gabbert, U., Ramos, R.R., Castillero, J.B., Díaz, R.G., 2007. Evaluation of effective material properties of randomly distributed short cylindrical fiber composites using a numerical homogenization technique. J. Mech. Mater. Struct. 2 (8), 1561–1570.

Chow, T.S., 1978. Effect of particle shape at finite concentration on the elastic modulus of filled polymers. J. Polym. Sci.: Polym. Phys. Ed. 16, 959–965.

Cook, R.D., Malkus, D.S., Plesha, M.E., Witt, R.J., 2002. Concept and Application of Finite Element Analysis. John Wiley & Sons Inc, New York.

Doghri, I., Tinel, L., 2005. Micromechanical modeling and computation of elasto–plastic materials reinforced with distributed-orientation fibers. Int. J. Plast. 21, 1919–1940.

Duschlbauer, D., Böhm, H.J., Pettermann, H.E., 2006. Computational simulation of composites reinforced by planar random fibres: Homogenization and localization by unit cell and mean field approaches. J. Compos. Mater. 40, 2217–2234.

Eckschlager, A., Böhm, H.J., Han, W., 2002. Multi-inclusion unit cell models for metal matrix composites with randomly oriented discontinuous reinforcements. Comput. Mater. Sci. 25, 42–53.

Eshelby, J.D., 1957. The determination of the elastic field of an ellipsoidal inclusion, and related problems. Proc. R. Soc. London A 241, 376–396.

Fu, S.Y., Lauke, B., 1996. Effect of fiber length and fiber orientation distributions on the tensile strength of short-fiber-reinforced polymers. Compos. Sci. Technol. 56, 1179–1190.

Ghossein, E., Lévesque, M., 2012. A fully automated numerical tool for a comprehensive validation of homogenization models and its application to spherical particles reinforced composites. Int. J. Solids Struct. 49, 1387–1398.

Gitman, I.M., Askes, H., Sluys, L.J., 2007. Representative volume: existence and size determination. Eng. Fract. Mech. 74, 2518–2534.

Halpin, J.C., 1969. Stiffness and expansion estimates for oriented short fiber composites. J. Compos. Mater. 3, 732–734.

Halpin, J.C., Kardos, J.L., 1976. The Halpin–Tsai equations: A review. Polym. Eng. Sci. 16 (5), 344–352.

Harris, B., 1999. Engineering Composite Materials. The Institute of Materials, London.

Hashin, Z., Rosen, B.W., 1964. Elastic moduli of fiber reinforced materials. J. Appl. Mech. 31, 223–232.

Hermans, J.J., 1967. The elastic properties of fiber reinforced materials when the fibers are aligned. Proc. R. Acad. Amsterdam B70. 1-

Hill, R., 1964. Theory of mechanical properties of fibre-strengthened materials: I. elastic behaviour. J. Mech. Phys. Solids 12, 199–212.

Hollister, S.J., Kikuchi, N., 1992. A comparison of homogenization and standard mechanics analyses for periodic porous composites. Comput. Mech. 10, 73–95.

Hori, M., Nemat-Nasser, S., 1999. On two micromechanics theories for determining micro-macro relations in heterogeneous solids. Mech. Mater. 31, 667–682.

Ionita, A., Weitsman, Y.J., 2006. On the mechanical response of randomly reinforced chopped-fibers composites: data and model. Compos. Sci. Technol. 66, 2566–2579.

Iorga, L., Pan, Y., Pelegri, A., 2008. Numerical characterization of material elastic properties for random fiber composites. J. Mech. Mater. Struct. 3 (7), 1279–1298.

Jain, A., Lomov, S.V., Abdin, Y., Verpoest, I., Paepegem, W.V., 2013. Pseudo-grain discretization and full Mori–Tanaka formulation for random heterogeneous media: predictive abilities for stresses in individual inclusions and the matrix. Compos. Sci. Technol. 87, 86–93.

Kanit, T., N'Guyen, F., Forest, S., Jeulin, D., Reed, M., Singleton, S., 2006. Apparent and effective physical properties of heterogeneous materials: Representativity of samples of two materials from food industry. Comput. Methods Appl. Mech. Eng. 195, 3960–3982.

Kari, S., Berger, H., Gabbert, U., 2007. Numerical evaluation of effective material properties of randomly distributed short cylindrical fibre composites. Comput. Mater. Sci. 39 (1), 198–204.

Kerner, E.H., 1956. The elastic and thermo-elastic properties of composite media. Proc. Phys. Soc. B 69, 808–813.

Mohite, P. M.,. Composite materials and structures. http://www.nptel.ac.in/courses/101104010/24.

Mori, T., Tanaka, K., 1973. Average stress in matrix and average elastic energy of materials with misfitting inclusions. Acta Metallurgica 21, 571–574.

Mura, T., 1987. Micromechanics of Defects in Solids. Kluwer Academic Publishers.

Nazarenko, L., Stolarski, H., Altenbach, H., 2016. Effective properties of short-fiber composites with Gurtin-Murdoch model of interphase. Int. J. Solids Struct. 97–98, 75–88.

Ogierman, W., Kokot, G., 2016. A study on fiber orientation influence on the mechanical response of a short fiber composite structure. Acta. Mech. 227, 173–183.

Pan, Y., Iorga, L., Pelegri, A.A., 2008a. Numerical generation of a random chopped fiber composite RVE and its elastic properties. Compos. Sci. Technol. 68, 2792–2798.

Pan, Y., Iorga, L., Pelegri, A.A., 2008b. Analysis of 3D random chopped fiber reinforced composites using FEM and random sequential adsorption. Comput. Mater. Sci. 43, 450–461.

Park, J.M., Park, S.J., 2011. Modeling and simulation of fiber orientation in injection molding of polymer composites. Math. Probl. Eng.. Article ID 105637:14

Pelissou, C., Baccou, J., Monerie, Y., Perales, F., 2009. Determination of the size of the representative volume element for random Quasi-brittle composites. Int. J. Solids Struct. 46 (14–15), 2842–2855.

Rezaei, F., Yunus, R., Ibrahim, N.A., 2009. Effect of fiber length on thermomechanical properties of short carbon fiber reinforced polypropylene composite. Mater. Des. 30, 260–263.

Russel, W.B., 1973. On the effective moduli of composite materials: effect of fiber length and geometry at dilute concentrations. J. Appl. Math. Phys. (ZAMP) 24, 581–600.

Schneider, P.J., Eberly, D.H., 2002. Geometric Tools for Computer Graphics, The Morgan Kaufmann Series in Computer Graphics and Geometric Modeling. Morgan Kaufmann Publishers.

Seidel, G.D., Lagoudas, D.C., 2006. Micromechanical analysis of the effective elastic properties of carbon nanotube reinforced composites. Mech. Mater. 38, 884–907.

Soden, P.D., Hinton, M.J., Kaddour, A.S., 1998. Lamina properties, lay-up configurations and loading conditions for a range of fibre-reinforced composite laminates. Compos. Sci. Technol. 58 (7), 1011–1022.

Sukiman, M.S., Kanit, T., N'Guyen, A., Imad, A., Moumen, E., Erchiqui, F., 2017. Effective thermal and mechanical properties of randomly oriented short and long fiber composites. Mech. Mater. 107, 56–70.

Tucker, C.L., Liang, E., 1999. Stiffness predictions for unidirectional short-fiber composites: review and evaluation. Compos. Sci. Technol. 59 (5), 655–671.

Velmurugan, R., Srinivasulu, G., Jayasankar, S., 2014. Influence of fibre waviness on the effective properties of discontinuous fiber reinforced composites. Comput. Mater. Sci. 91, 339–349.

Vincent, M., Giroud, T., Clarke, A., Eberhardt, C., 2005. Description and modeling of fiber orientation in injection molding of fiber reinforced thermoplastics. Polym 46, 6719–6725.